Strength distribution of large unidirectional composite patches with realistic load sharing

Ankit Gupta, Sivasambu Mahesh,* and Shyam M. Keralavarma

Department of Aerospace Engineering,

Indian Institute of Technology Madras, Chennai 600 036, India.

Abstract

Monte-Carlo simulations of the failure of unidirectional fibre composites in a plane transverse to the fibre direction are performed on much larger patches than in previous works, assuming a realistic load redistribution scheme from broken to intact fibres. Computational effort involved in these simulations is substantially reduced using a novel algorithm based on the quadtree data structure. The empirical strength distribution obtained from the simulations has a weak-link character, regardless of the variability in fibre strengths. The empirical strength distribution is well-captured by a probabilistic model based on the growth of a tight cluster of fibre breaks. It is also well-captured by regarding composite patch failure as the failure of the weakest equal load sharing bundle of a certain size, following W. A. Curtin, Phys. Rev. Lett. 80, 1445 (1998). The approximate coincidence of these two predictions identifies the dominant failure mechanism underlying Curtin's empirical scaling relationship.

PACS numbers: 72.80.Tm, 02.50.Ey, 02.70.ac, 05.10.Ln

* Corresponding author: smahesh@iitm.ac.in

I. INTRODUCTION

I.1. Fibre strength distribution

The strength of a chain of links connected in series equals the strength of the weakest link. Let the chain be comprised of n_{link} links, whose random strengths Σ_i, $i \in \{1, 2, \ldots, n_{\text{link}}\}$ are independent and identically distributed following the power law, $\Pr\{\Sigma_i \leq \sigma\} = (\sigma/\sigma_0)^\rho$, for $\sigma \leq \sigma_0$, a reference link strength. The strength of the chain is then distributed as

$$F(\sigma) = \Pr\left\{\min_{i\in\{1,2,\ldots,n\}} \Sigma_i \leq \sigma\right\} = 1 - \exp\left(-n_{\text{link}}\left(\frac{\sigma}{\sigma_0}\right)^\rho\right). \tag{1}$$

Weibull [1] showed that the distribution function $F(\sigma)$ fits a number of empirically distributions very well, sometimes even when there was no obvious physical basis resembling the chain of links argument. The Weibull distribution, Eq. (1), is commonly used to describe fibre strength [2].

The case of links arranged in parallel and collectively sustaining the applied load proves to be considerably more complex [3]. In this case, the load sharing, i.e., the pattern of load redistribution from broken to intact fibres, becomes important. Two extremes of load sharing can be immediately identified: equal load sharing (ELS), and local load sharing (LLS).

I.2. Equal load sharing

In equal load sharing (ELS), the load dropped by a broken fibre is equally distributed amongst the intact fibres in that cross-section. Thus, in a parallel system comprised of N fibres, if N_b fibres were broken, the stress concentration in the remaining $N - N_b$ intact fibres would be

$$K_{\text{els}} = N/(N - N_b). \tag{2}$$

Equal load sharing applies to a loose bundle of threads, not embedded in a matrix. The strength distribution of such bundles was studied by Daniels [4], who showed that the bundle strength of an equal load sharing system is Gaussian distributed in the limit $N \to \infty$. Let σ be the stress per fibre in a bundle, i.e., the total applied load divided by NA_f, where A_f denotes the fibre cross-sectional area. Let $G_{\text{ELS}}(\sigma)$ denote the probability that the bundle

strength per fibre is no greater than σ. Then,

$$G_{\mathrm{ELS}}(\sigma) = \Phi(\sigma; \mu, s_N) = \frac{1}{s_N\sqrt{2\pi}} \int_{-\infty}^{\sigma} \exp\left\{\frac{-(t-\mu)^2}{2s_N^2}\right\} dt, \quad \text{where,} \tag{3a}$$

$$\mu = \sigma_\tau[1 - F(\sigma_\tau)], \quad \text{and} \quad s_N^2 = \sigma_\tau^2 F(\sigma_\tau)[1 - F(\sigma_\tau)]/N. \tag{3b}$$

Here, $\sigma_\tau = \max_\sigma\{\sigma[1-F(\sigma)]\}$, and $\Phi(\sigma; \mu, s_N)$ denotes the Gaussian cumulative distribution function with mean μ and standard deviation s_N [4].

Eq. (3) turns out to be an excellent approximation for bundle strength for about $N \geq 50$. For equal load sharing bundles with smaller N, the following recursive expressions, due to McCartney and Smith [5], yield a better approximation for bundle strength, $G_{\mathrm{ELS}}(\sigma; N)$. For convenience, the ELS bundle strength obtained recursively is denoted $E^{(N)}(\sigma)$, and is expressed as:

$$E^{(N)}(\sigma) = \{F(\sigma'_{N-1})\}^N - \sum_{m=0}^{N-1} \binom{N}{m} \Pi^{(m)} \{F(\sigma'_{N-1}) - F(\sigma'_m)\}^{N-m}. \tag{4}$$

In Eq. (4), $F(\cdot)$ is given by Eq. (1),

$$\Pi^{(m)} = \{F(\sigma'_{m-1})\}^m - \sum_{n=0}^{m-1} \binom{m}{n} \Pi^{(n)} \{F(\sigma'_{m-1}) - F(\sigma'_n)\}^{m-n},$$

$\binom{m}{n} = m!/(n!(m-n)!)$, $\sigma'_k = N\sigma/(N-k)$, and $\Pi^{(0)} = 1$.

I.3. Local load sharing

In local load sharing (LLS), the load dropped by each broken fibre is distributed amongst its nearest intact neighbours [6, 7]. This severely localises the overload due to broken fibres. Let K_l denote the greatest LLS stress concentration ahead of a cluster of l breaks, for $l \in \{1, 2, \ldots\}$. If the variance in fibre strength is small, as characterised by a large ρ in Eq. (1), the most overloaded fibre sitting in the perimeter of a cluster of fibre breaks is highly likely to fail, as $F(K_l\sigma) \gg F(\sigma)$. The insight that for large ρ, the probability of failure of the most overloaded fibre is much greater than that of any other fibre was used by Smith [6], Smith *et al.* [7], and Harlow and Phoenix [8, 9] to construct a stochastic model of failure for 1- and 2-dimensional local load sharing composites. In this model, composite failure is identified with the occurrence of the weakest of N independent and identically distributed failure events, each obeying the distribution $W_{\mathrm{LLS}}(\sigma)$, where N is the number of

fibres. Thus, for large ρ, the using a weakest-link argument similar to that used to derive Eq. (1), the composite strength distribution is given by

$$\begin{aligned} G_{\mathrm{LLS}}(\sigma) &= 1 - (1 - W_{\mathrm{LLS}}(\sigma))^N \\ &\approx 1 - \exp\left(-NW_{\mathrm{LLS}}(\sigma)\right). \end{aligned} \tag{5}$$

The approximation in Eq. (5) is valid for small $W_{\mathrm{LLS}}(\sigma) \ll 1$. It is noticed that Eq. (5) for a parallel system has the same form as Eq. (1), which applies to a serial system. For this reason, in the limit $\rho \to \infty$, $G_{\mathrm{LLS}}(\sigma)$ is said to have a weakest-link character described by the strength distribution of the weakest link, $W_{\mathrm{LLS}}(\sigma)$.

The difference in the characteristics of the strength distributions, Eqs. (3) and (5), respectively, corresponding to ELS and LLS with large ρ arises from differences in their respective failure modes. The failure of an ELS composite patch occurs by global fibre breakage, whereas the failure of an LLS patch comprised of fibres with large ρ occurs by the growth of a cluster of breaks. In the nomenclature of Curtin [10], ELS patches are termed 'tough', while large ρ LLS patches are said to be 'brittle'.

The probability that the most overloaded fibre adjacent to a single break, or adjacent to a small cluster of l breaks fails, becomes increasingly independent of its stress concentration K_l as $\rho \to 0$, because $\lim_{\rho\to 0} K_l^\rho = 1$, and $\lim_{\rho\to 0} F(K_l\sigma) = F(\sigma)$. Therefore, for small ρ (say, $\rho < 5$), a small cluster of breaks is highly unlikely to extend by failing the most overloaded intact fibre abutting it. However, for any fixed $\rho > 0$, there must exist a sufficiently large cluster of L breaks such that $F(K_L\sigma) \gg F(\sigma)$. Such a cluster will extend by breaking the most overloaded intact fibre abutting it with high probability. This qualitative argument suggests that LLS composites must fail in a brittle manner also for small ρ, provided such a cluster forms in the first place. Furthermore, it suggests that the minimum size L of a cluster of breaks capable of propagating as a crack must increase with decreasing ρ.

The conclusion that LLS composite failure has a brittle character has been reached rigorously in several special cases. Through a transition matrix based analysis, in one-dimensional 0-1 composites and fuse-network models, Harlow [11] and Duxbury and Leath [12] demonstrated the brittle character of composite and network failure, respectively. Mahesh and Phoenix [13] showed the absence of the brittle ductile transition in a one-dimensional composite model with power-law distributed fibre strengths. Also, Kahng *et al.* [14] demonstrated brittle failure for the case of a two-dimensional resistor-fuse network, with fuse

burn-out voltages following a uniform distribution, in the limit of a large network.

The foregoing arguments prompt the following questions: (i) How does the minimum cluster size capable of catastrophic propagation, L, scale with ρ, and σ and (ii) What is the statistically most important mechanism underlying the formation of the L-cluster of breaks for fixed, but not necessarily large ρ.

In the case of two-dimensional composite patches with Weibull distributed fibre strengths, Habeeb and Mahesh [15] used Monte-Carlo simulations on large local load sharing composite patches to answer the foregoing questions. They showed that the strength distribution of a local load sharing bundle has a weakest-link character for all ρ. They also identified the dominant failure event for all ρ, and estimated the probability of its occurrence. The most significant deviation between their stochastic model, and that of Smith *et al.* [7] lies in the definition of the elementary failure event. Whereas in Smith *et al.* [7], the elementary events in the growth of clusters are the breakages of fibres abutting the cluster, in Habeeb and Mahesh [15], the elementary failure events are the failure of appropriately sized ELS sub-bundles. In the limit of large ρ, the stochastic model of Habeeb and Mahesh [15] collapses into that of Smith *et al.* [7], as the number of fibres in the ELS sub-bundles approaches one.

I.4. Hedgepeth load sharing

Neither the equal nor the local load sharing models is realistic for a typical polymer matrix composite [2]. While the load redistribution due a fibre break in these composites is localised, the localisation is not as severe as in the local load sharing model. In reality, more distant fibres than just the nearest neighbours experience an overload due to a broken fibre. A realistic model of load sharing in a cross-sectional plane of unidirectional polymer matrix composites is due to Hedgepeth [16] and Hedgepeth and Van Dyke [17].

One way to place the Hedgepeth load sharing model (HLS) in between the ELS and LLS models is to consider the asymptotic rate of decay of the stress overload with distance, r from a single break, for large r. Asymptotic stress decay in ELS and LLS composites correspond to r^0 and $r^{-\infty}$, respectively. The asymptotic overload decay rate for the HLS model is r^{-3} in 2-dimensions [18]. The qualitative argument made to show that LLS composites are brittle also applies to HLS, so that HLS composite failure must also be brittle. Again, the size scaling of the minimum critical size with ρ and σ and the dominant mechanism of formation

of a cluster of this size remain open questions, particularly in the regime of small ρ. As in LLS, in this regime, small clusters of breaks cannot be expected to extend by failing their most overloaded intact neighbours.

Monte Carlo simulations of HLS patches, reported by Mahesh *et al.* [19], comprised of up to $N = 900$ fibres show weakest-link scaling of the empirical strength distribution for $\rho \geq 3$:

$$G_{\mathrm{HLS}}(\sigma) = 1 - (1 - W_{\mathrm{HLS}}(\sigma))^N \approx 1 - \exp\left(-NW_{\mathrm{HLS}}(\sigma)\right). \tag{6}$$

For $\rho < 3$, however, the weakest-link scaling appears to break down. Instead, the empirical strength distributions appear to approach the Gaussian distribution given by Eq. (3) with decreasing ρ. This result suggests a qualitative transition in the character of the composite strength distribution 'brittle' character at large ρ to 'tough' character for small ρ. The observed transition though is an artefact of the limited patch size of the simulations. If the spatial extent of the weakest-link event were comparable to, or larger than the composite patch size, the empirical strength distribution will not reflect its true weakest-link character. Because of this limitation, simulations in Mahesh *et al.* [19] cannot conclusively answer the open questions noted in the preceding paragraph.

Curtin [20], on the basis of Monte Carlo simulations of composite patches with up to $N = 2500$ fibres, and $\rho \geq 3$, found that the strength distribution of HLS bundles has a weakest-link character. Furthermore, he found that their empirical strength distribution satisfies

$$G_{\mathrm{HLS}}(\sigma) = 1 - \left\{1 - \Phi(\sigma; \mu', s_{N_c'})\right\}^{N/N_c'}, \tag{7}$$

where $\Phi(\cdot)$ denotes the Gaussian cumulative distribution function of Eq. (3), μ' is a fitting parameter, and $1 \leq N_c' \leq N$ is another. Eq. (7) implies that the N-fibre HLS composite patch may be regarded as a collection of N/N_c' non-overlapping bundles, each comprised of N_c' fibres. The failure of any of these sub-bundles causes composite failure. The surprising aspect of this observation is that the bundle strengths are Gaussian distributed, and the standard deviation, $s_{N_c'}$ coincides with that given in Eq. (3). Unfortunately, a conceptual explanation of the scaling relation, Eq. (7), is presently unavailable. Eq. (7) has also only been established empirically for HLS bundles for $\rho \geq 3$. It is known [15] that LLS bundles do not obey the scaling of Eq. (7).

I.5. Detailed load sharing models

As noted above, the HLS model is more realistic than either the ELS or LLS models of a polymer matrix composite. However, certain predictions of the HLS model have been found to be in discord with experimental measurements. For example, HLS predicts the stress concentration on the intact fibre next to a break to be independent of the inter-fibre spacing. Experimentally, however, stress concentrations are found to depend on inter-fibre spacing [21]. This discrepancy between HLS and experiment can be attributed to the matrix carrying some tensile load in the physical composite, an aspect neglected by the HLS model. To account for such deviations, more detailed shear lag models have been developed in the literature, e.g.,[22–25]. These models account more realistically for the tensile load carried by the elastoplastic matrix, and debonding/sliding fibre matrix interface. The effects of matrix yielding and cracking, deviations from a regular lattice of fibre placement, staggering of breaks out of a transverse plane, etc. have also received considerable attention in recent years, e.g.,[26–29]. The more realistic representation of the composite structure and load transfer in the aforementioned models comes at a much greater computational cost. Monte Carlo simulations on these more realistic models must therefore be limited to much smaller patch sizes than those treated using HLS. Simulations of large patches using these realistic models is therefore presently infeasible.

Realistic modelling of the matrix and interfacial typically blunts a crack, i.e., distributes the load dropped by broken fibres over a wider range. The load transfer predicted by HLS is more localised. For this reason, composite strength predicted assuming the HLS model can be expected to be conservative. The computational efficiency of the HLS model, and its conservative overestimation of stress concentrations, make it best suited for computationally studying the failure of large patches presently.

I.6. Scope of the present work

It is clear from the foregoing survey that Monte Carlo simulations are an important tool to gain understanding of the statistics of composite patches. It is also clear that failure simulations of larger composite patches than studied in the literature are needed in order to capture the weakest-linking characteristics at small ρ. Accordingly, Monte-

Carlo simulations are performed in large two-dimensional composite patches with up to $2^{16} = 65536$ fibres. Load redistribution from broken to intact fibres at every step of these simulations is computed using a novel tree based algorithm, which reduces the computational effort of the simulations by more than an order of magnitude. The novel algorithm is described in Sec. II.3.

The present simulation results, reported in Sec. III, show that HLS composites fail in a brittle fashion for all ρ. The dominant failure mode of the composite for all ρ is identified, and a simple stochastic model, combining elements of the models of Smith *et al.* [7], Mahesh *et al.* [19] and Habeeb and Mahesh [15] is developed in Sec. III.3. The model captures the empirical weakest-link strength distribution obtained from the Monte Carlo simulations well. The present empirical strength distributions also obey the scaling relationship, Eq. (7), due to Curtin [20]. The coincidence of the predictions identifies the dominant failure event underlying the scaling relationship of Curtin [20].

II. THE MODEL COMPOSITE

II.1. Governing equations and the unit break solution

The greatest volume fraction of identical cylindrical fibres in a unidirectional composite is obtained by arranging them in a hexagonal lattice. Accordingly, fibre centres are presently assumed to be located at the points of a hexagonal lattice, as shown in Fig. 1. The cross-section of the composite patch is itself taken to be rhombus shaped. This cross-section contains $N = \nu^2$ fibres. Two edges of the rhombus define the m, and n coordinate axes. To avoid edge effects, the following periodicity conditions are imposed: fibers $(0, n)$ and $(\nu-1, n)$ (the left and right edges of the patch) are assumed adjacent for all $n \in \{0, 1, \ldots, \nu - 1\}$. Similarly, fibers at the top $(n = \nu-1)$ and bottom $(n = 0)$ edges for all $m \in \{0, 1, \ldots, \nu-1\}$ are also considered adjacent.

Following Hedgepeth and Van Dyke [17], each fibre is assumed to interact with its six neighbours. Let ζ be the non-dimensional fibre-wise position, and let $u_{m,n}(\zeta)$ denote the normalised displacement of fibre (m, n) in the fibre direction. Then, the equilibrium equation of fibre (m, n) reads as [17]

$$\frac{d^2 u_{m,n}}{d\zeta^2} - 6u_{m,n} + u_{m+1,n} + u_{m-1,n} + u_{m,n+1} + u_{m,n-1} + u_{m+1,n-1} + u_{n-1,m+1} = 0. \qquad (8)$$

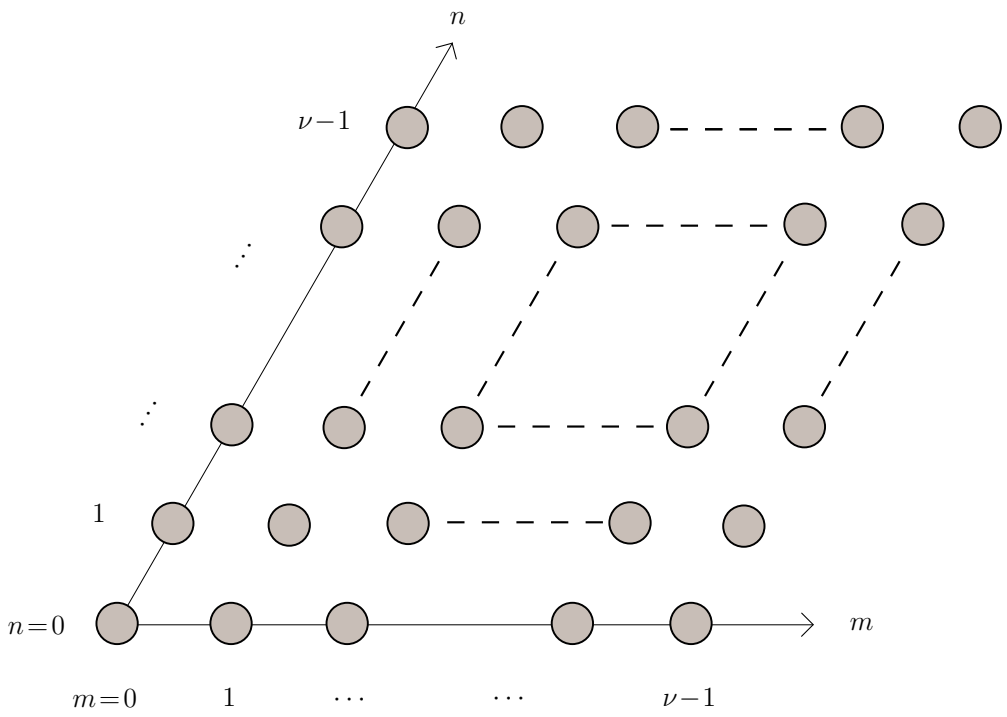

FIG. 1: A rhombus-shaped periodic patch of $N = \nu \times \nu$ fibres arranged in a hexagonal lattice. A periodic tiling of the plane by such patches is used to represent a cross-section of the composite. The m–n coordinate system is also shown.

Consider the case of the composite loaded under unit far-field strain, and containing a single fibre break located at $m = 0$, $n = 0$ in the cross-section $\zeta = 0$ under consideration. The corresponding boundary conditions are:

$$\begin{aligned} \frac{du_{0,0}}{d\zeta}(\zeta = 0) &= 0, \\ u_{m,n}(\zeta = 0) &= 0, \quad \text{for all } m \neq 0,\ n \neq 0; \\ \frac{du_{m,n}}{d\zeta}(\zeta = \pm\infty) &= 1, \quad \text{for all } m, n. \end{aligned} \tag{9}$$

The above boundary value problem was formulated with periodic boundary conditions by Landis *et al.* [30] and solved for the unknown functions $u_{m,n}(\zeta)$. Recently, a fast algorithm for its solution was proposed by Gupta *et al.* [18]. The periodic boundary conditions endow the solution with the property of translation invariance. That is, if the single break were located at $(m, n) = (m^*, n^*)$ instead of at $(m, n) = (0, 0)$, the displacement of the fibre at

(m, n) would be given by $u_{\Delta m, \Delta n}(\zeta)$, where

$$\begin{aligned} \Delta m &= (m - m^*) \bmod \nu, \quad \text{and} \\ \Delta n &= (n - n^*) \bmod \nu. \end{aligned} \tag{10}$$

Let the fibre located at (m, n) be identified by the index $k = m\nu + n + 1$. The overload on this fibre due to the broken fibre at (m^*, n^*), identified by the index $l = m^*\nu + n^* + 1$, is termed the overload coefficient between fibres k and l. It is defined as

$$\lambda_{kl} = \frac{du_{\Delta m, \Delta n}}{d\zeta}(\zeta = 0) - 1. \tag{11}$$

Eq. (11) indicates that the translation invariance of $u_{m,n}(\zeta)$ carries over to λ_{kl} also. The overload coefficient is symmetric, i.e., $\lambda_{kl} = \lambda_{lk}$, and satisfies $\lambda_{kl} > 0$ if $k \neq l$. An important property of λ_{kl}, which amounts to demanding equilibrium at the cross-section $\zeta = 0$ is that

$$\sum_{\substack{l=1 \\ l \neq k}}^{N} \lambda_{kl} = 1, \quad \text{for all } k. \tag{12}$$

Two important numerical properties of λ_{kl}, used in the sequel are [31]:

$$\min_{k \in \{1,2,\ldots,N\}} \lambda_{kl} = \lambda_{ll} = -1, \text{ and } \max_{k \in \{1,2,\ldots,N\}} \lambda_{kl} \approx 0.1046. \tag{13}$$

II.2. Interacting multiple breaks

Interactions between multiple breaks in the transverse section $\zeta = 0$ follows the break influence superposition scheme, developed by Hedgepeth [16], Sastry and Phoenix [32], and Beyerlein *et al.* [33]. Suppose that the N_b fibres with indices $\{k_1, k_2, \ldots, k_{N_b}\}$ are broken in the plane $\zeta = 0$. Each broken fibre, k_i, $i \in \{1, 2, \ldots, N_b\}$ is associated with a weight $w_{k_i} \geq 1$, which physically signifies its normalised opening displacement [33]. The opening displacements, and hence the weights of intact fibres are identically zero. The condition of zero traction at all the breaks then requires that [16, 32, 33]

$$\sum_{j=1}^{N_b} \lambda_{k_i k_j} w_{k_j} = -1, \quad \text{for all } i \in \{1, 2, \ldots, N_b\}, \tag{14}$$

or, in matrix notation as:

$$[\lambda]\{w\} = -\{1\}. \tag{15}$$

Here, $[\lambda]$ is an $N_b \times N_b$ square matrix whose ij-th entry is $\lambda_{k_i k_j}$, and $\{1\}$ denotes an N_b column vector of ones. Expressed as a matrix, $[\lambda]$ has the following useful properties for $N_b < N$, and $i, j \in \{1, 2, \ldots, N_b\}$: (i) negative unit diagonals: $\lambda_{k_i k_i} = -1$, (ii) positive off-diagonals: $\lambda_{k_i k_j} > 0$, for $i \neq j$, (iii) symmetry: $\lambda_{k_i k_j} = \lambda_{k_j k_i}$, and (iv) diagonal dominance:

$$\sum_{\substack{j=1 \\ j \neq i}}^{N_b} |\lambda_{k_i k_j}| < |\lambda_{k_i k_i}|, \quad \text{for } \; 1 \leq i \leq N_b. \tag{16}$$

By virtue of these properties, the matrix $-[\lambda]$ is symmetric positive definite [34, Def. 1.20 and Cor. 1.22]. With the weights of the broken fibres evaluated, the overloads Ω_k on all the fibres, k, whether broken or intact, is given by a weighted superposition of the overload coefficients as:

$$\Omega_k = \sum_{j=1}^{N_b} \lambda_{k k_j} w_{k_j}, \quad \text{for all } k \in \{1, 2, \ldots, N\}. \tag{17}$$

Cholesky decomposition is the most efficient direct method for the solution of Eq. (15). It entails a computational cost of $O(N_b^3)$, and memory requirement of $O(N_b^2)$. The matrix-vector product in Eq. (17) entails a further computational cost of $O(N N_b)$. For large N, and N_b, of the order of tens of thousands, these computational expenses become prohibitive.

It is known that λ_{kl} of Eq. (11) decays as the inverse cubic power of the Euclidean distance between fibre k and the from the broken fibre, l [18, 35]. This rapid rate of decay is exploited next to substantially reduce the computational effort and computer memory needed to solve Eq. (15), and to obtain the overloads using Eq. (17).

II.3. Tree method

II.3.1. Quadtree representation of the composite patch

Consider again, the $N = \nu^2$ fibre patch of Fig. 1, where $\log_2 \nu = \log_4 N$ is an integer. Thus, $\nu \in \{1, 2, 4, 8, 16, \ldots\}$. A $\nu = 16$ composite patch is shown in Fig. 2. The entire patch is subdivided into four equal sub-regions, each comprised of $(\nu/2)^2$ fibres, as shown in Fig. 2a. These parts are further sub-divided similarly, until a stage is reached where all the finest sub-regions are comprised of only one fibre. At this stage, no further sub-division is possible.

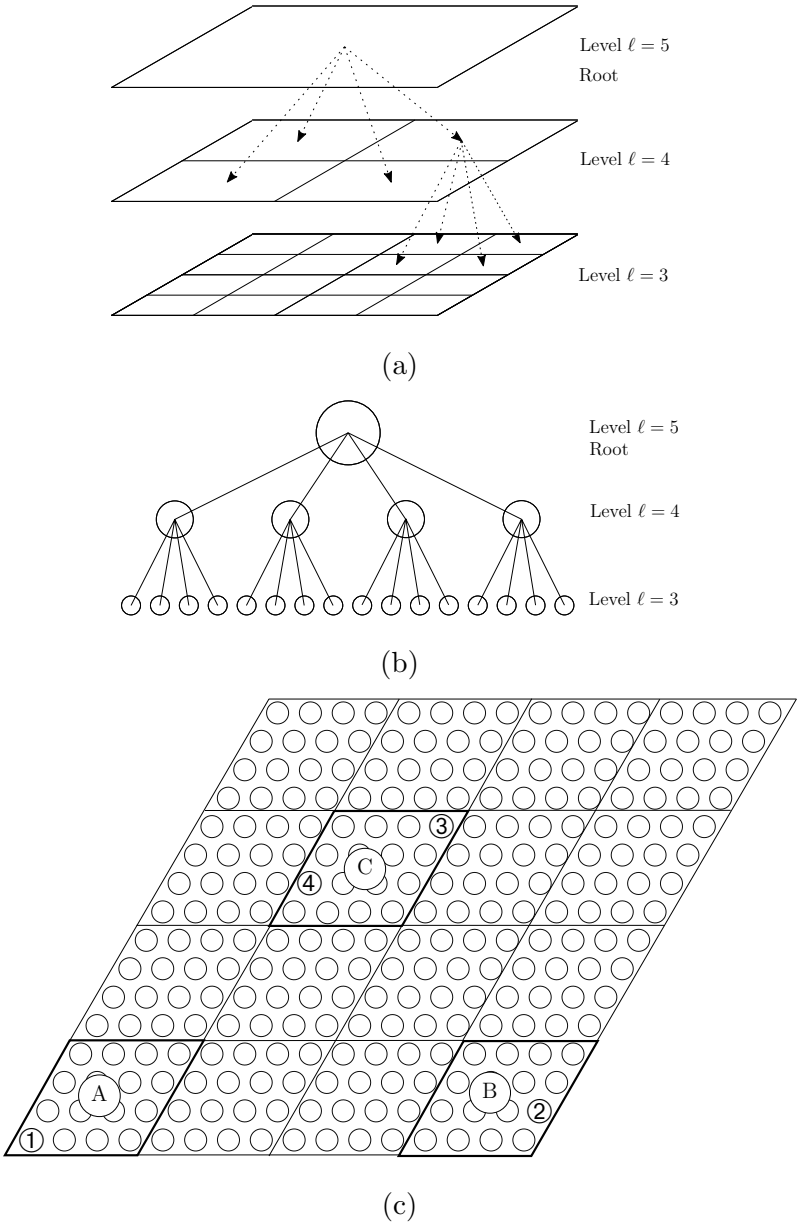

FIG. 2: (a) Hierarchical sub-division of the composite patch into sub-regions, shown to three levels. The lowest two levels of this tree, $\ell = 1, 2$, are not shown. (b) A quadtree representation of the subdivision, also limited to $\ell = 3, 4$, and 5. (c) The $N = 16^2$ fibre composite patch showing the subdivision of level $\ell = 3$.

The hierarchical subdivision is best represented by a quadtree data structure [36], sketched in Fig. 2b. Each sub-region is represented in the quadtree as a node. Nodes are depicted as circles in Fig. 2b. In the following, nodes are distinguished by enclosing their identifier within square braces, e.g., node $[a]$. The symbol $[r]$ is reserved to denote

the root node. The root node occupies the highest level of the quadtree, and represents the entire domain of the composite patch. The four children of $[r]$ form the next lower level. The sixteen children of these nodes occupy the even lower level, and so on. A tree representing N fibres has $L := 1 + \log_4 N$ levels. These levels are numbered sequentially from the bottom to the top. Fig. 2 shows only the levels $3, 4$, and 5 of the quadtree. The level of node $[a]$ is denoted $\ell_{[a]}$.

Consider a typical node $[a]$. Its four children are denoted $[a_1]$, $[a_2]$, $[a_3]$, and $[a_4]$. The unique parent of node $[a]$ is denoted $[P_{[a]}]$. Also, the unique ancestor of node $[a]$ in level ℓ is defined if $\ell \geq \ell_{[a]}$. It is denoted $[P^{(\ell)}_{[a]}]$. It is convenient for algorithmic reasons to assume that $[P^{(\ell)}_{[a]}] = [a]$, if $\ell = \ell_{[a]}$. Nodes at the lowest level $\ell = 1$ of the quadtree represent fibres and are termed leaves. Node numbers of leaf nodes are taken to coincide with the fibre index. Thus, fibre k is represented in the tree by node $[k]$. The set of all nodes descended from node $[a]$, and contained in level ℓ are denoted $\mathscr{D}^{(\ell)}_{[a]}$, e.g., $\mathscr{D}^{(1)}_{[r]}$ is the set of all the leaf nodes in the quadtree.

II.3.2. Nearby and distant node pairs

The overload experienced by fibre k due to a break at $\zeta = 0$ in fibre l, λ_{kl} was defined in Eq. (11). Presently, an analogous overload coefficient, $\Lambda_{[a][b]}$, between a pair of nodes $[a]$ and $[b]$ is developed.

Consider two nodes $[a] \in \mathscr{D}^{(\ell)}_{[r]}$ and $[b] \in \mathscr{D}^{(\ell)}_{[r]}$, at level ℓ. Let

$$\begin{aligned} \overline{\lambda}_{[a][b]} &= \max_{\{[k']\in\mathscr{D}^{(1)}_{[a]}\}} \max_{\{[l']\in\mathscr{D}^{(1)}_{[b]}\}} \lambda_{k'l'}, \text{ and} \\ \underline{\lambda}_{[a][b]} &= \min_{\{[k']\in\mathscr{D}^{(1)}_{[a]}\}} \min_{\{[l']\in\mathscr{D}^{(1)}_{[b]}\}} \lambda_{k'l'} \end{aligned} \tag{18}$$

denote the maximum and minimum overloads, respectively, produced by a break amongst any of the fibres in $\mathscr{D}^{(1)}_{[b]}$ on any of the intact fibres in $\mathscr{D}^{(1)}_{[a]}$. From the symmetry of $\lambda_{k'l'}$, and from Eq. (18), it follows that $\overline{\lambda}_{[a][b]} = \overline{\lambda}_{[b][a]}$, and $\underline{\lambda}_{[a][b]} = \underline{\lambda}_{[b][a]}$.

Nodes $[a]$ and $[b]$ are considered distant if

$$\Theta_{[a][b]} := 1 - \left\{ \underline{\lambda}_{[a][b]} \,/\, \overline{\lambda}_{[a][b]} \right\} \leq \theta, \tag{19}$$

where $\theta \in [0, 1)$ is a preset parameter. Otherwise, nodes $[a]$ and $[b]$ are considered nearby.

If nodes $[a]$ and $[b]$ are distant, and if none of their ancestors are distant, i.e., if

$$\Theta_{[P_{[a]}^{(\ell')}][P_{[b]}^{(\ell')}]} > \theta, \quad \text{for all } \ell' \in \{\ell+1, \ell+2, \ldots, L\}, \tag{20}$$

then nodes $[a]$ and $[b]$ are assigned a non-zero overload coefficient, $\Lambda_{[a][b]}$:

$$\Lambda_{[a][b]} = f(\underline{\lambda}_{[a][b]}, \overline{\lambda}_{[a][b]}). \tag{21}$$

$f(\underline{\lambda}_{[a][b]}, \overline{\lambda}_{[a][b]})$ in Eq. (21) must satisfy the reciprocal relationship

$$f(\underline{\lambda}_{[a][b]}, \overline{\lambda}_{[a][b]}) = f(\underline{\lambda}_{[b][a]}, \overline{\lambda}_{[b][a]}). \tag{22}$$

The specific form of $f(\underline{\lambda}_{[a][b]}, \overline{\lambda}_{[a][b]})$, which is henceforth referred to as the smearing function, is developed in Appendix A. If either Eq. (19) and/or Eq. (20) is not true, or if $\ell_{[a]} \neq \ell_{[b]}$, $\Lambda_{[a][b]}$ is set to zero. In summary,

$$\Lambda_{[a][b]} = \begin{cases} f(\underline{\lambda}_{[a][b]}, \overline{\lambda}_{[a][b]}), & \text{if } \ell_{[a]} = \ell_{[b]}, \text{ and if Eqs. (19) and (20) are true,} \\ 0, & \text{otherwise.} \end{cases} \tag{23}$$

The matrix $[\Lambda]$, whose ab-th element is $\Lambda_{[a][b]}$, is sparse [37]. Its sparsity will be exploited in the numerical method described in Sec. II.3.5 below.

Intuitively, if $[a]$ and $[b]$ are distant nodes, it is expected that $\overline{\lambda}_{[a][b]} \approx \underline{\lambda}_{[a][b]}$. Since $\underline{\lambda}_{[a][b]} \leq \lambda_{k'l'} \leq \overline{\lambda}_{[a][b]}$, the overload coefficients $\lambda_{k'l'}$, for all the fibres k' and l' in the sub-regions represented by the nodes $[a]$ and $[b]$, will be similar in value. In this case, $\Lambda_{[a][b]}$ of Eq. (21) represents the smeared overload produced in the fibres of node $[a]$ due to a single break located amongst the fibres of node $[b]$:

$$\Lambda_{[a][b]} \approx \lambda_{k'l'}, \quad \text{for all } k' \in \mathscr{D}_{[a]}^{(1)}, \text{ and } l' \in \mathscr{D}_{[b]}^{(1)}. \tag{24}$$

However, if $[a]$ and $[b]$ are nearby nodes, such an approximation will be unreasonably erroneous. Eq. (23) formalises these intuitive notions.

II.3.3. Smeared overload coefficients, $\tilde{\lambda}_{kl}$

Consider a pair of fibres, k and l. According to the convention established in Sec. II.3.1, these are represented in the quadtree by the nodes $[k]$ and $[l]$. The set

$$\left\{ \Lambda_{[P_{[k]}^{(\ell)}][P_{[l]}^{(\ell)}]} : \ell \in \{1, 2, \ldots, L\} \right\} \tag{25}$$

contains exactly one non-zero element. All other elements of the set given in Eq. (25) must be zero, since Eqs. (19) and (20) may be simultaneously satisfied only for a unique level, say, $\ell = \ell^*_{kl}$. Define

$$\tilde{\lambda}_{kl} := \Lambda_{\left[P^{(\ell^*_{kl})}_{[k]}\right]\left[P^{(\ell^*_{kl})}_{[l]}\right]} = \sum_{\ell=1}^{L} \Lambda_{\left[P^{(\ell)}_{[k]}\right]\left[P^{(\ell)}_{[l]}\right]}. \tag{26}$$

This definition, together with Eq. (24) then imply:

$$\lambda_{kl} \approx \tilde{\lambda}_{kl}. \tag{27}$$

$\tilde{\lambda}_{kl}$ is uniform-valued over sub-regions represented by the higher nodes of the tree:

$$\tilde{\lambda}_{k'l'} = \tilde{\lambda}_{kl}, \quad \text{for all } k' \in \mathscr{D}^{(1)}_{\left[P^{(\ell^*_{kl})}_{[k]}\right]} \text{ and } l' \in \mathscr{D}^{(1)}_{\left[P^{(\ell^*_{kl})}_{[l]}\right]}. \tag{28}$$

Therefore, $\tilde{\lambda}_{kl}$ may be thought to be a smeared version of $\lambda_{k'l'}$. Smearing allows the aggregation of interactions between distant collections of breaks, which will underlie the greater computational efficiency of the tree method in Sec. II.3.5.

Consider the special case $k = l$, corresponding to the self-interaction of a fibre k. Clearly, $\lambda_{kk} = \underline{\lambda}_{[k][k]} = \overline{\lambda}_{[k][k]}$ and from Eq. (19), $\Theta_{[k][k]} = 0$. The condition of Eq. (19) thus passes for any $\theta \in [0, 1)$. Also, for any $\ell > 1$ in Eq. (20), invoking Eq. (13), $\Theta_{[P^{(\ell)}_{[k]}][P^{(\ell)}_{[k]}]} = 1 - (-1/0.1046) > 1 > \theta$, for any $\theta \in [0, 1)$. It follows that $\Lambda_{[k][k]} = \lambda_{kk} = -1$. The set of Eq. (25) now becomes $\{-1, 0, 0, \ldots, 0\}$. Therefore, $\ell^*_{kk} = 1$ and

$$\tilde{\lambda}_{kk} = -1, \tag{29}$$

according to Eq. (26).

Two fibres, k and l, interact directly if $\ell^*_{kl} = 1$, and indirectly if $\ell^*_{kl} > 1$. Direct and indirect interactions are distinguished by defining

$$D_{kl} = \begin{cases} \tilde{\lambda}_{kl}, & \text{if } \ell^*_{kl} = 1, \text{ and} \\ 0, & \text{if } \ell^*_{kl} > 1, \end{cases} \tag{30}$$

and

$$H_{kl} = \begin{cases} 0, & \text{if } \ell^*_{kl} = 1, \text{ and} \\ \tilde{\lambda}_{kl}, & \text{if } \ell^*_{kl} > 1. \end{cases} \tag{31}$$

II.3.4. Interaction between fibre breaks

Consider again, a set of interacting breaks, $\{k_1, k_2, \ldots, k_{N_b}\}$, as in Sec. II.2. Recalling $[\lambda]$ from Eq. (15), approximating $\lambda_{k_i k_j} \approx \tilde{\lambda}_{k_i k_j}$, and writing $\tilde{\lambda}_{k_i k_j} = D_{k_i k_j} + H_{k_i k_j}$ results in

$$[\lambda] \approx [\tilde{\lambda}] = [D] + [H], \tag{32}$$

where, $[\tilde{\lambda}]$, $[D]$ and $[H]$ are $N_b \times N_b$ square matrices whose ij-th elements are $\tilde{\lambda}_{k_i k_j}$, $D_{k_i k_j}$ and $H_{k_i k_j}$, respectively.

The decomposition, Eq. (32), is illustrated for the composite patch depicted in Fig. 2c. Four fibres, say ①, ②, ③, and ④, are shown broken. The corresponding leaf nodes are denoted [①], [②], [③], and [④]. The division of the composite patch into sub-regions of level $\ell = 3$ is also shown. Nodes $[A]$, $[B]$, and $[C]$ contain the fibre breaks; $[P^{(3)}_{[①]}] = [A]$, $[P^{(3)}_{[②]}] = [B]$, and $[P^{(3)}_{[③]}] = [P^{(3)}_{[④]}] = [C]$.

Taking $\theta = 0.7$, it is found that Eqs. (19) and (20) are satisfied only for the interactions between the distinct node pairs $([①],[②])$, $([③],[④])$, $([A],[C])$ and $([B],[C])$. Interactions between other higher level nodes do not occur, as they violate Eqs. (19) and/or (20). In terms of the interactions between higher nodes, the approximate coefficient matrix, $[\tilde{\lambda}]$ is

$$\begin{bmatrix} \tilde{\lambda}_{[①][①]} & \tilde{\lambda}_{[①][②]} & \tilde{\lambda}_{[①][③]} & \tilde{\lambda}_{[①][④]} \\ \tilde{\lambda}_{[②][①]} & \tilde{\lambda}_{[②][②]} & \tilde{\lambda}_{[②][③]} & \tilde{\lambda}_{[②][④]} \\ \tilde{\lambda}_{[③][①]} & \tilde{\lambda}_{[③][②]} & \tilde{\lambda}_{[③][③]} & \tilde{\lambda}_{[③][④]} \\ \tilde{\lambda}_{[④][①]} & \tilde{\lambda}_{[④][②]} & \tilde{\lambda}_{[④][③]} & \tilde{\lambda}_{[④][④]} \end{bmatrix} = \begin{bmatrix} \Lambda_{[①][①]} & \Lambda_{[①][②]} & \Lambda_{[A][C]} & \Lambda_{[A][C]} \\ \Lambda_{[②][①]} & \Lambda_{[②][②]} & \Lambda_{[B][C]} & \Lambda_{[B][C]} \\ \Lambda_{[C][A]} & \Lambda_{[C][B]} & \Lambda_{[③][③]} & \Lambda_{[③][④]} \\ \Lambda_{[C][A]} & \Lambda_{[C][B]} & \Lambda_{[④][③]} & \Lambda_{[④][④]} \end{bmatrix}. \tag{33}$$

The left side of Eq. (33) shows the interaction matrix of all four breaks with each other. The right side can be split as

$$\begin{aligned} \begin{bmatrix} \Lambda_{[①][①]} & \Lambda_{[①][②]} & \Lambda_{[A][C]} & \Lambda_{[A][C]} \\ \Lambda_{[②][①]} & \Lambda_{[②][②]} & \Lambda_{[B][C]} & \Lambda_{[B][C]} \\ \Lambda_{[C][A]} & \Lambda_{[C][B]} & \Lambda_{[③][③]} & \Lambda_{[③][④]} \\ \Lambda_{[C][A]} & \Lambda_{[C][B]} & \Lambda_{[④][③]} & \Lambda_{[④][④]} \end{bmatrix} &= \begin{bmatrix} \Lambda_{[①][①]} & \Lambda_{[①][②]} & 0 & 0 \\ \Lambda_{[②][①]} & \Lambda_{[②][②]} & 0 & 0 \\ 0 & 0 & \Lambda_{[③][③]} & \Lambda_{[③][④]} \\ 0 & 0 & \Lambda_{[④][③]} & \Lambda_{[④][④]} \end{bmatrix} \\ &+ \begin{bmatrix} 0 & 0 & \Lambda_{[A][C]} & \Lambda_{[A][C]} \\ 0 & 0 & \Lambda_{[B][C]} & \Lambda_{[B][C]} \\ \Lambda_{[C][A]} & \Lambda_{[C][B]} & 0 & 0 \\ \Lambda_{[C][A]} & \Lambda_{[C][B]} & 0 & 0 \end{bmatrix}, \\ &= [D] + [H]. \end{aligned} \tag{34}$$

All interactions between nearby fibre breaks feature in $[D]$, while those between distant fibre breaks appear in $[H]$.

II.3.5. Iterative numerical method

Writing Eq. (14), using Eq. (32) as

$$-[\lambda]\{w\} \approx -\left([D]+[H]\right)\{w\} = \{1\}, \tag{35}$$

suggests the following iterative scheme:

$$-[D]\{w\}^{\iota} = \{1\} + [H]\{w\}^{\iota-1}, \tag{36}$$

where ι is the iteration counter. Iterations are initialised by taking $\{w\}^{\iota=0} = \{1\}$. By construction, $-[D]$ is diagonal dominant with positive diagonal entries. Therefore, it is positive definite. By construction, $[-D]$ is also a sparse matrix, as all indirect interactions are not represented in $-[D]$. Therefore, $\{w\}^{\iota}$ can be computed by conducting one iteration of the conjugate gradient algorithm [37, 38], exploiting the sparsity of $-[D]$. Prior to the next iteration, $\iota+1$, it is necessary to update the overloads on all broken fibres due to distant breaks. This overload is given by $\sum_{j=1}^{N_b} H_{k_i k_j} w_{k_j}^{\iota}$, for all $i \in \{1, 2, \ldots, N_b\}$.

Fortunately, it is neither necessary to store $[H]$ in computer memory, nor to perform a computationally expensive matrix vector multiplication for this purpose. Instead, the weights of all higher nodes ($\ell > 1$) of the quadtree are simply set to the sum of the weights of their four children:

$$w_{[a]}^{\iota} = w_{[a_1]}^{\iota} + w_{[a_2]}^{\iota} + w_{[a_3]}^{\iota} + w_{[a_4]}^{\iota}. \tag{37}$$

Recursively performing this update starting from the root node [39] sets the weights, $w_{[a]}^{\iota}$, for all quadtree nodes, $[a] \in \cup_{\ell=2}^{L} \mathscr{D}_{[r]}^{(\ell)}$. Eq. (37) involves the transfer of node weights up the quadtree from the fibres to the root. Using $w_{[a]}^{\iota}$, the overloads due to distant breaks on the node $[b]$, $\Omega_{[b]}^{\iota,H}$, can be recursively computed as:

$$\Omega_{[b]}^{\iota,H} = \begin{cases} \Omega_{\left[P_{[b]}\right]}^{\iota,H} + \sum_{\{[a]\in\mathscr{D}_{[r]}^{\ell_{[b]}}\}} \Lambda_{[b][a]} w_{[a]}^{\iota}, & \text{if } \ell_{[b]} > 1, \\ \Omega_{\left[P_{[b]}\right]}^{\iota,H}, & \text{if } \ell_{[b]} = 1. \end{cases} \tag{38}$$

The first case of Eq. (38) accounts for the overload on a non-leaf node $[b]$, as the sum of contributions from still higher nodes, and contributions from other nodes at level $\ell_{[b]}$.

Overloads engendered by direct interactions between fibres are not from distant breaks. The second case of Eq. (38), therefore, excludes such contributions on leaf nodes $[b]$. With $\Omega^{\iota,H}_{[b]}$ defined as in Eq. (38),

$$\sum_{j=1}^{N_b} H_{k_i k_j} w^{\iota}_{k_j} = \Omega^{\iota,H}_{[k_i]}. \tag{39}$$

The residual at the ι-th iteration is given by

$$\{R\}^{\iota} = -[D]\{w\}^{\iota+1} - [H]\{w\}^{\iota+1} - \{1\}. \tag{40}$$

The iterations are terminated when $\|\{R\}^{\iota}\|/\|\{1\}\| < \varepsilon$, a preset tolerance. The matrix splitting $[\lambda] \approx ([D] + [H])$ is a regular splitting in the terminology of Varga [34]. This property guarantees convergence of the iterative scheme of Eq. (36) provided $-([D] + [H])$ is symmetric and positive definite [34, Th.3.31]. The latter condition has been ensured by construction.

Finally, attention is turned to computing the overloads in intact fibres due to an arbitrary distribution of breaks, with known weights, w_{k_i}, $i \in \{1, 2, \ldots, N_b\}$. Recursively applying Eq. (38) on all the nodes of the quadtree beginning with the root, $[r]$, yields the overloads due to distant nodes in all the fibres, broken, or otherwise [39]. The overload at a leaf node $[k]$ representing fibre k is the sum of overloads produced by distant and nearby fibre breaks:

$$\Omega^{\iota}_{[k]} = \Omega^{\iota,H}_{[k]} + \sum_{\{[l] \in \mathscr{D}^{(1)}_{[r]}\}} \Lambda_{[k][l]} w^{\iota}_{[l]}. \tag{41}$$

Let a typical fibre directly interact with N' fibres. Typically for large patches, $N' \ll N$. The second term in Eq. (41) then involves $N'N_b$ non-zero products, which is considerably smaller than the cost of evaluating the overloads using Eq. (17) directly. Sparsity of $[\Lambda]$, noted previously in Sec. II.3.3 is used in evaluating Eq. (41) in the present implementation [38].

III. RESULTS

III.1. Penny-shaped fibre break clusters

The accuracy and efficiency of the tree algorithm of Sec. II.3 is first evaluated, using penny-shaped clusters of breaks in a large periodic composite patch as test cases. In the tests, the patch is comprised of $N = 2^{16} = 65536$ fibres. Accuracy is evaluated by comparing

the tree predicted overloads ahead of the penny-shaped clusters, with those predicted by the exact calculation of Sec. II.2. Computational efficiency is measured by comparing the CPU times needed for the two computations.

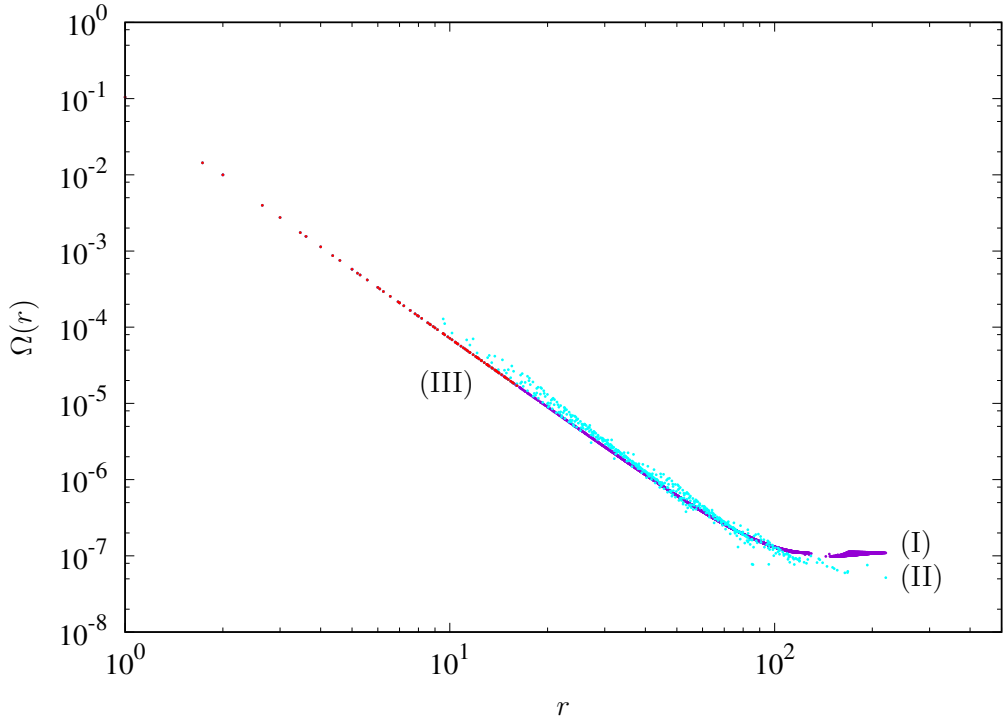

FIG. 3: Stress overloads, $\Omega(r)$, predicted ahead of a single fibre break in a patch comprised of $N = 2^{16}$ fibres. r is the Euclidean distance from the broken fibre. Predictions obtained from three calculations are shown: (I) Exact overload computation using Eq. (17); (II) Approximate overload computation using the tree method of Sec. II.3, taking $\theta = 0.5$; and (III) Overloads obtained by neglecting interactions between distant nodes. Distant node pairs are determined using Eq. (19) with $\theta = 0.5$.

Fig. 3 compares the stress overloads predicted both exactly, and using the tree method, ahead of a single break in a periodic patch comprised of $N = 2^{16}$ fibres. In this figure, r denotes the Euclidian distance of intact fibres from the single break, normalised by the centre-to-centre spacing between neighbouring fibres. Since there are no interacting breaks, the weight of the single broken fibre is unity. It is seen that the two methods predict similar overloads, although $\Omega(r)$ predicted using the tree method, shows more scatter. This is to be expected since the influence of the break is smeared uniformly (Sec. II.3.3) across nodes, representing many fibres in the tree method.

Fig. 3 also shows the overloads obtained by entirely neglecting interactions between distant nodes, by setting $[H] = [0]$ in Eq. (32). Since the boundary between nearby and distant nodes is located at $r \approx 15$, the overloads for $r > 15$ obtained by neglecting distant nodes are zero.

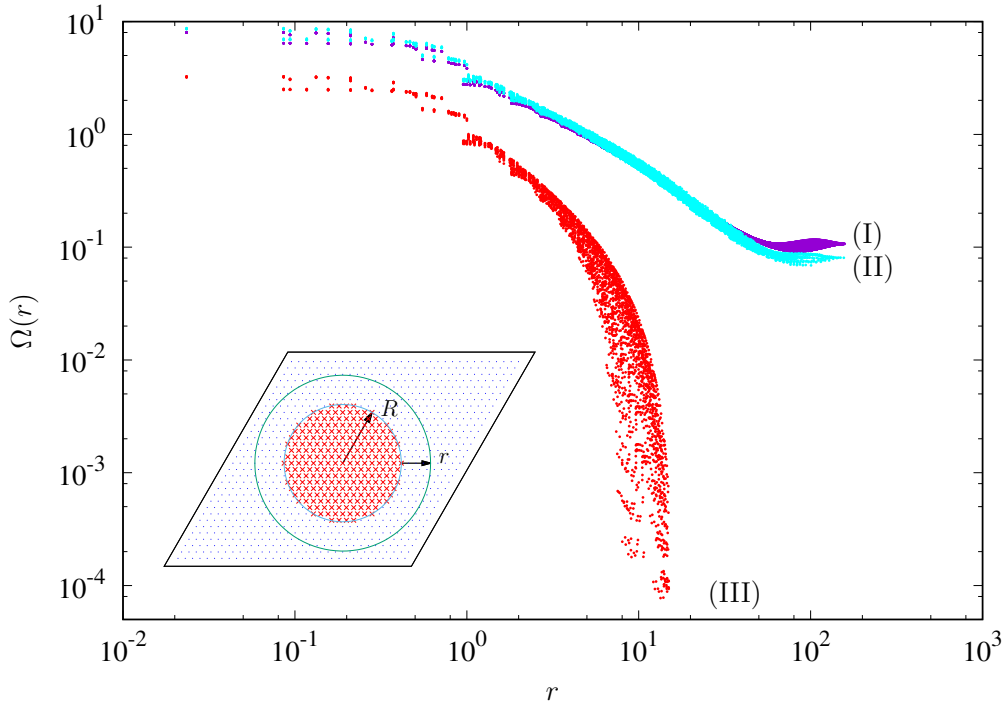

FIG. 4: Stress overloads, $\Omega(r)$, predicted ahead of a cluster of fibre breaks of radius $R = 2^6$ in a patch comprised of $N = 2^{16}$. r is the Euclidean distance from the cluster tip. Predictions obtained from three calculations are shown: (I) Direct solution of weights from Eq. (14) and overload computation using Eq. (17); (II) Solution using the tree method of Sec. II.3, taking $\theta = 0.5$; and (III) Direct solutions of weights neglecting all interactions between distant nodes. Distant node pairs are determined using Eq. (19) with $\theta = 0.5$.

Next, the stress overloads due to a large penny-shaped cluster of breaks, of normalised radius $R = 2^6$ is considered, as shown inset in Fig. 4. The number of fibre breaks in the penny-shaped cluster is $N_b = 14865$; more than a quarter of all fibres in the patch are broken. Let $R+r$ denote the Euclidean distance from the centre of the cluster to each intact fibre. In other words, subtracting R from the Euclidian distance of each intact fibre from the centre of the penny-shaped cluster yields the distance of the fibre from the crack tip, r. $R+r$, and r will usually not be integer-valued. For a number of intact fibres neighbouring the cluster of breaks, $r < 1$.

Fig. 4 compares the variation of the predicted stress overloads with r using both exact and tree methods. The overloads predicted by the two methods are found to agree reasonably well for all r; the greatest deviation occurs at $R + r \approx \nu$, i.e., near the boundary of the periodic patch. The tree method underestimates these overloads. The scatter in the overload levels for a given r is greater in the tree predictions than in the exact calculation, again on account of the smearing described in Sec. II.3.3, which is intrinsic to the tree approximation. Also shown in Fig. 4 are the overload predictions obtained by cutting off the influence of distant nodes, for $\theta = 0.5$. Doing so results in grossly underestimation of the overloads, especially at large r. This result emphatically shows that the influence of distant breaks should not be neglected.

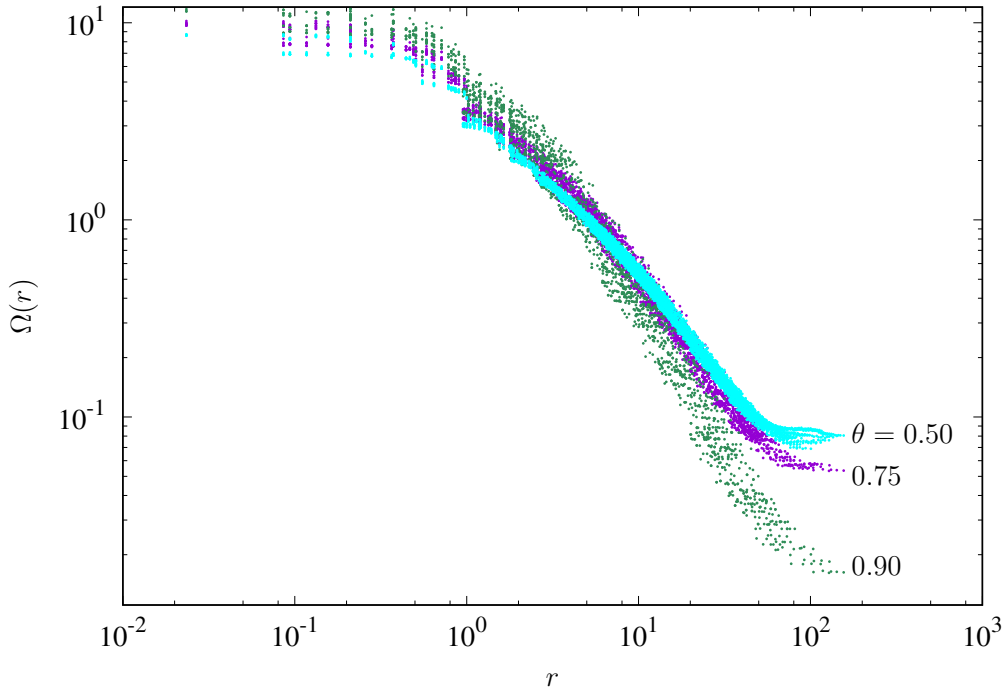

FIG. 5: Variation with θ of stress overloads predicted ahead of a penny shaped crack of radius, $R = 2^6$ in a composite patch with $N = 2^{16}$ fibres.

Fig. 5 shows the effect of increasing θ on the stress overloads ahead of an $R = 2^6$ cluster of breaks in an $N = 2^{16}$ patch. Increasing θ increases the scatter in the overload profiles. This is because with increasing θ, interactions between fibres becomes increasingly smeared over ever larger numbers of fibres. The scattered overloads predicted by $\theta = 0.5$, 0.75, and 0.90 overlap for about $r \leq 5$. At larger distances, the overloads predicted by $\theta = 0.9$ are systematically smaller than those predicted by the smaller θ. The effect of the patch edges

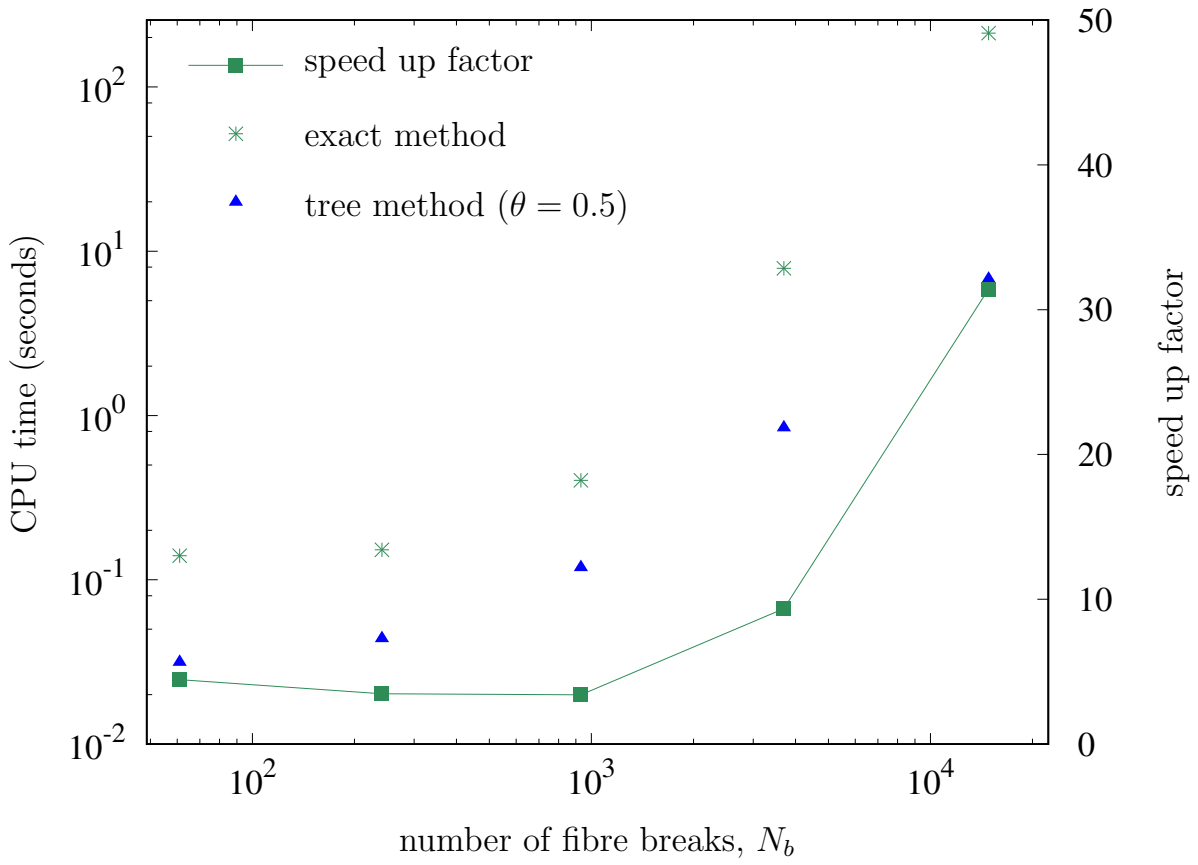

FIG. 6: CPU time required for calculating weights (a) by exactly solving Eq. (14), and (b) by the approximate tree method ($\theta = 0.5$). N_b is the number of fibres in a cluster of breaks. The radii of the clusters studied are $R = 2^2, 2^3, 2^4, 2^5$, and 2^6. The speed up factor is simply the ratio of the CPU times required for the exact calculation and the tree-based calculation.

thus extends substantially into the patch for the case of $\theta = 0.9$, than it does for $\theta = 0.5$ and 0.75.

The CPU time requirements for the computing the stress-overloads due to penny-shaped clusters of various radii $R = 2^2, 2^3, 2^4, 2^5$, and 2^6 by the exact and tree methods is shown in Fig. 6. N_b denotes the number of broken fibres in the penny-shaped cluster. Calculations for the tree method were performed taking $\theta = 0.5$. In all cases, computing the exact solution is more time consuming than computing using the tree method. For small N_b, the speed up obtained using the tree method, which is the ratio of the CPU times required for the exact calculation and the tree-based calculation, is relatively small. This is because the overheads associated with the recursive tree operations, e.g., evaluation of Eqs. (37) and (38), outweigh

any computational gains in solving Eq. (36) by the tree method. The computational cost associated with Eqs. (37) and (38) are fixed for all N_b. Therefore, the computational speed up increases with larger N_b. The computational speed up can be considerable. For example, corresponding to $R = 2^6$, the tree method is about 30 times faster than the exact calculation.

Since tree calculations assuming $\theta = 0.5$ give an acceptable approximation of the overloads, and since computational time is sufficiently reduced for $\theta = 0.5$, this value is used in all the Monte Carlo simulations reported below.

III.2. Monte Carlo simulations

Monte Carlo simulations of composite patch failure are performed on a wide range of composite sizes: $N = 2^8$, 2^{10}, 2^{12}, 2^{14}, and 2^{16}. For each size, the fibre strength Weibull exponents $\rho = 0.5$, 1, 2, 3, 5 and 10 have been simulated. For each N and ρ, $n_{\text{simul}} = 250$ simulations have been performed. The simulation algorithm follows that of Mahesh *et al.* [19, 31], except that the tree method of Sec. II.3 is used to update the fibre stresses (ratio of fibre load and fibre cross-sectional area) after the formation of new fibre breaks. Each simulation begins by assigning a strength drawn from the Weibull distribution, Eq. (1), to each of the N fibres. It is assumed that $\sigma_0 = 1$. The applied stress per fibre is raised to the point where exactly one fibre will break. Stress redistribution is computed using the tree method. If any other fibres will fail under the influence of the stress concentration of the first break, those fibres are also failed. Otherwise, the applied stress per fibre is incremented to the point of failing exactly one more fibre. This process is repeated until all the fibres fail. The applied stress per fibre is not allowed to decrease. The applied stress per fibre at which all the N fibres fail is the composite patch strength per fibre, and denoted σ_i, $i = 1, 2, \ldots, n_{\text{simul}}$. The composite strengths, sorted in ascending order, are denoted $\sigma_{(i)}$, $i = 1, 2, \ldots, n_{\text{simul}}$. Empirical strength distributions are deduced from this data. The value of the empirical cumulative distribution function assigned to $\sigma_{(i)}$ is

$$G_{\text{emp}}(\sigma_{(i)}) = \frac{i}{n_{\text{simul}} + 1}, \qquad \text{for all } i = 1, 2, \ldots, n_{\text{simul}}. \tag{42}$$

The variation of the applied stress per fibre over the simulation history for the weakest ($(i) = 1$) $\rho = 1$, $N = 2^{10} = 1024$ composite patch is plotted in Fig. 7a. A large number of applied stress increments are performed and 590 fibres break before the remaining fibres fail

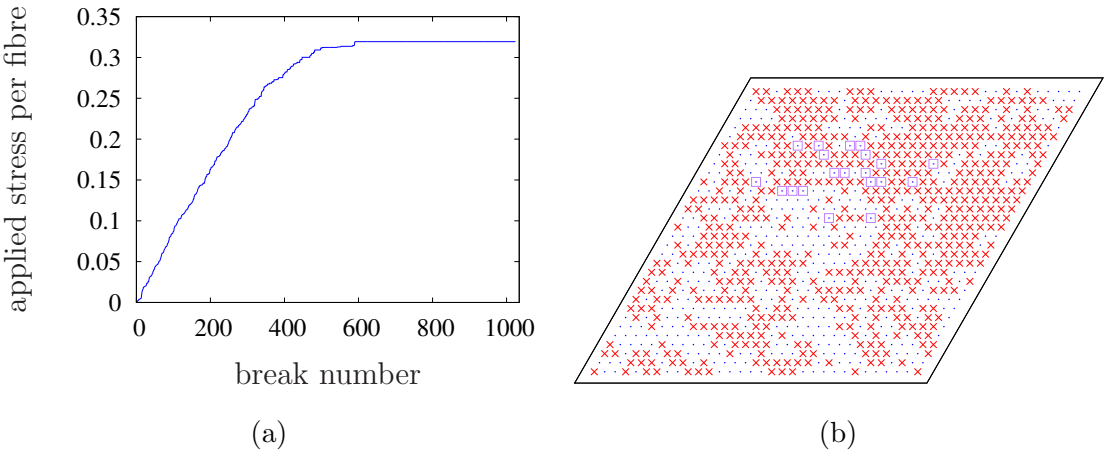

(a) (b)

FIG. 7: (a) Evolution of the applied stress per fibre with the number of fibre breaks, in the weakest ($(i) = 1$) of 250 Monte Carlo simulations for a composite patch comprised of $N = 2^{10}$ fibres with Weibull exponent $\rho = 1$. (b) Intact fibres (blue dots), broken fibres at the instant when the peak applied stress is first reached (red crosses), and the first twenty fibres that fail after the peak load is reached (blue squares), are shown.

under the influence of the overloads due to the existing fibre breaks. The fibres that break before the peak load is attained, and the first twenty fibres that break at the peak load are indicated in Fig. 7b.

In the weakest $\rho = 10$ specimen, as shown in Fig. 8a, only thirteen fibres break before the applied stress reaches its peak value. Many of these breaks are isolated, as shown in Fig. 8b. However, a cluster of breaks forms near the upper/lower edges of the patch, which propagates catastrophically at the peak load. It is recalled that the upper and lower edges are equivalent because of the assumed periodicity.

These simulations on small composite patches suggest that $\rho = 10$ patches are 'brittle', while $\rho = 1$ patches are 'tough', following the nomenclature introduced in Sec. I.3. However, this suggestion is on account of the small patch size. A qualitatively different picture emerges from the simulations of large patches, described below.

Paralleling Eq. (6), consider the empirical weakest-link distribution:

$$W_{\text{emp}}(\sigma_{(i)}; \rho, N) = 1 - (1 - G_{\text{emp}}(\sigma_{(i)}; \rho))^{1/N}. \tag{43}$$

Fig. 9 plots the empirical $W_{\text{emp}}(\sigma_{(i)}; \rho, N)$ deduced from simulations of the composite patches of all sizes N and all ρ studied presently. For clarity, the abscissa is normalised by the

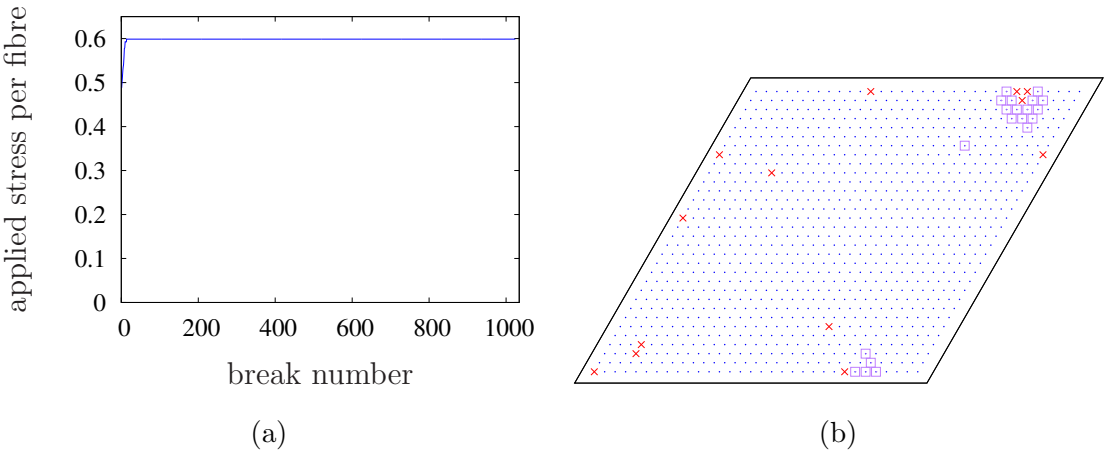

(a) (b)

FIG. 8: (a) Evolution of the applied stress per fibre with the number of fibre breaks, in the weakest ($(i) = 1$) of 250 Monte Carlo simulations for a composite patch comprised of $N = 2^{10}$ fibres with Weibull exponent $\rho = 10$. (b) Intact fibres (blue dots), broken fibres at the instant when the peak applied stress is first reached (red crosses), and the first twenty fibres that fail after the peak load is reached (blue squares), are shown.

mean fibre strength, $\mu_F = \Gamma(1 + 1/\rho)$. Without this normalisation, the $W_{\text{emp}}(\sigma_{(i)}; \rho, N)$ distributions for some of the ρ cross each other. It is clear that for each $\rho \geq 1$, there exists a critical patch size, $N_c(\rho)$ such that $W_{\text{emp}}(\sigma_{(i)}; \rho, N)$ becomes independent of N for $N \geq N_c(\rho)$, i.e.,

$$W_{\text{emp}}(\sigma_{(i)}; \rho, N) = W_{\text{emp}}(\sigma_{(i)}; \rho), \text{ for } N \geq N_c(\rho). \tag{44}$$

It is also clear that the critical $N_c(\rho)$ decreases with increasing ρ. For $\rho = 10$, the empirical weakest-link distribution of even the smallest simulated patch, $N = 2^8$, already obeys Eq. (44). This implies that $N_c(\rho = 10) < 2^8$. For $\rho = 1$, however, $N = 2^8$ and $N = 2^{10}$ do not obey Eq. (44), but $N \geq 2^{12}$ does. Thus, $2^{10} < N_c(\rho = 1) \leq 2^{12}$. For $\rho = 0.5$, Eq. (44) is approached, but not yet reached even for $N_c = 2^{14}$. But it appears that simulating even larger patches will lead to Eq. (44) being followed for some $N_c(\rho = 0.5) \geq 2^{14}$. Inverting the foregoing argument, no matter how large the simulated composite patch size, N, there will be a small enough ρ, for which Eq. (44) cannot be directly demonstrated using Monte Carlo simulations, on account of the simulation patch size being inadequate. This is a limitation of the simulations. It does not imply a break down of Eq. (44) for low ρ.

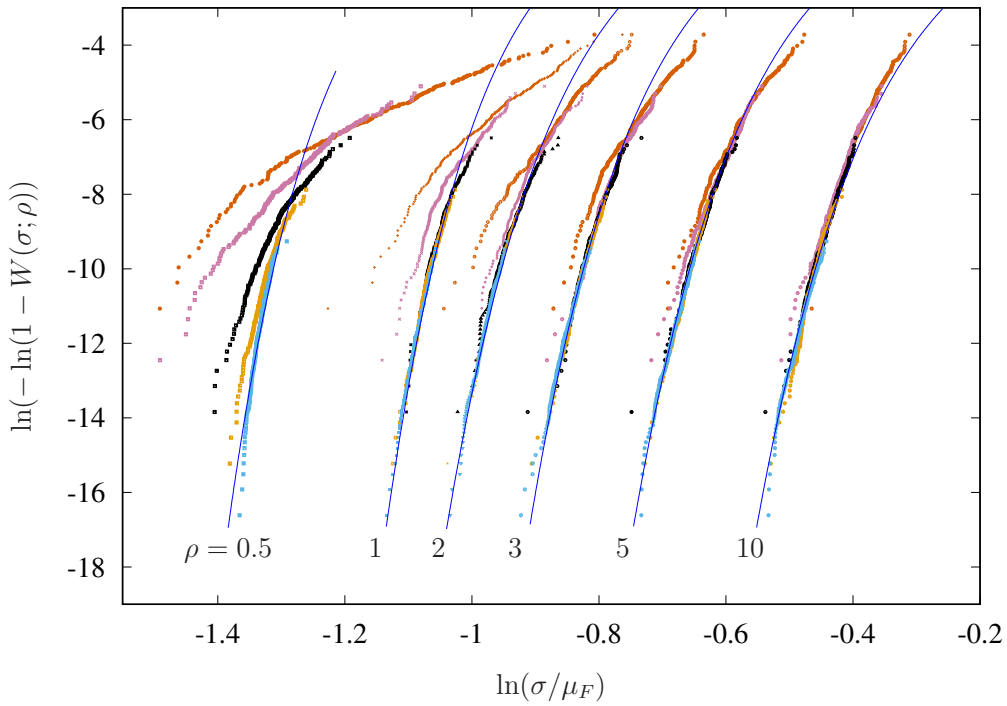

FIG. 9: Empirical weakest-link distribution functions, $W_{\text{emp}}(\sigma;\rho,N)$, obtained from 250 Monte Carlo simulations, for each value of Weibull exponent $\rho \in \{0.5, 1, 2, 3, 5, 10\}$, and for patch sizes, $N \in \{2^8, 2^{10}, 2^{12}, 2^{14}, 2^{16}\}$. Vermilion, purple, black, orange and blue dots, correspond respectively to these patch sizes. The blue lines correspond to fits obtained using the simple stochastic model of Sec. III.3.

III.3. Probabilistic 'tight' cluster growth model

As noted in Sec. I.3, Smith *et al.* [7] proposed a dominant failure event, whose occurrence underlies the weakest-link strength distribution for LLS bundles with large ρ. The proposed failure event ceases to be dominant at smaller ρ. A dominant failure event for all ρ was proposed by Habeeb and Mahesh [15] by introducing the failure of equal load sharing (ELS) bundles as the elementary events in the chain of events leading up to LLS composite patch failure. Presently, the latter 'tight' cluster growth model is adapted for Hedgepeth load sharing (HLS).

The dominant failure event proposed by Smith *et al.* [7], viz., 'tight' cluster growth, involves the sequential failure of the most overloaded neighbouring fibres. This is illustrated in Fig. 10 for Hedgepeth load sharing (HLS). The failure of a fibre maximally overloads its $N_1 = 6$ neighbours equally, as shown in Fig. 10a. The failure of any of these fibres maximally

(a)

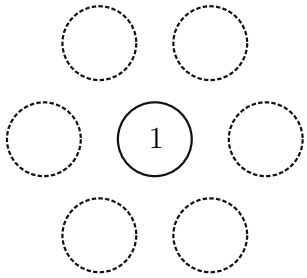

$\Omega_1 = 0.1046$

$N_1 = 6$

(b)

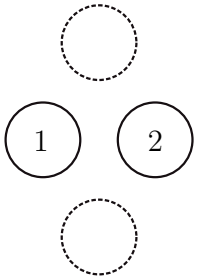

$\Omega_2 = 0.2336$

$N_2 = 2$

(c)

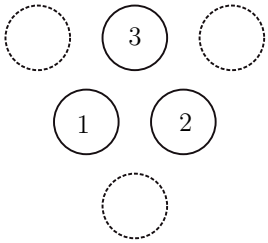

$\Omega_3 = 0.2826$

$N_3 = 3$

FIG. 10: Overloads, Ω_P, and number of most overloaded fibres, N_P, around a 'tight' cluster of (a) $P = 1$, (b) $P = 2$, and (c) $P = 3$ fibres broken in a tight cluster. The applied load is taken to be unity.

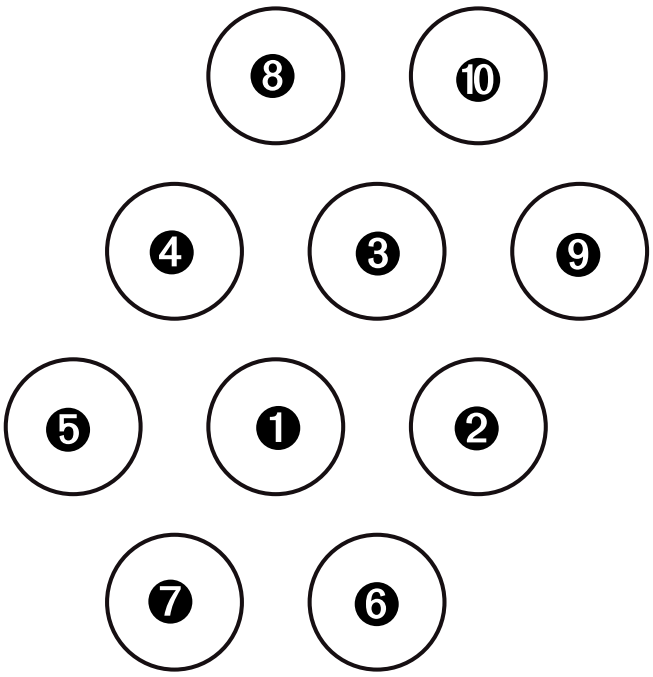

P	Ω_P	N_P
0	0.0000	0
1	0.1046	6
2	0.2336	2
3	0.2826	3
4	0.3203	4
5	0.3641	2
6	0.5385	1
7	0.4102	6
8	0.4590	2
9	0.6156	1
10	0.5051	4

(a)

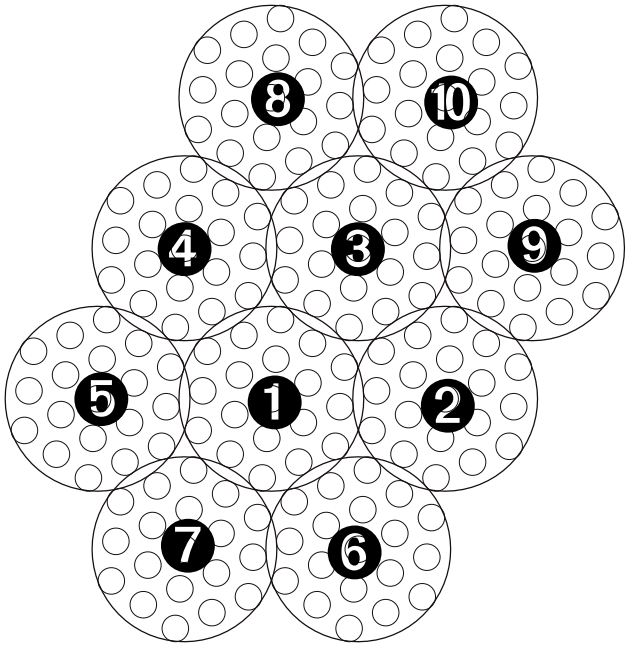

(b)

FIG. 11: (a) Progression of fibre breakage leading to a 'tight' cluster of $P = 10$ breaks. Overloads Ω_P and number of most overloaded neighbours N_P of the P cluster, are also tabulated. Note the non-monotonicity in Ω_P and N_P, with cluster size, P. (b) Progression of failure of ELS M-bundles, leading to 'tight' cluster growth of the crack, analogous to (a). $M = 19$, as shown. In (a), and (b), ❶, ❷, ... indicate the order of fibre, and M-bundle breakage, respectively.

overloads two of the neighbours of the cluster of breaks, as shown in Fig. 10b. Failure of one of the two most severely overloaded neighbours produces the failure configuration of Fig. 10c, overloading three of the neighbours most severely. Continuing this process of failing one of the most severely overloaded fibres, tight cluster growth is obtained. The development of a tight cluster of ten breaks is illustrated in Fig. 11. Also listed are the overloads, Ω_P and the number of most overloaded neighbouring fibres, N_P around a tight cluster of P breaks, for $P \in \{1, 2, \ldots, 10\}$, as predicted by HLS.

'Tight' cluster growth in the present model of composite failure follows that of Smith *et al.* [7], with the exception that failure of single fibres in the original model is replaced with that of ELS bundles comprised of M fibres, termed M-bundles. The schematic development of a tight cluster of broken M-bundles, for $M = 19$, is shown in Fig. 11b. For the case that $M = 1$, the present tight cluster growth model reduces to that of Smith *et al.* [7].

Recalling from Eq. (4) that $E^{(M)}(\sigma)$ denotes the strength distribution of an equal load sharing bundle of M fibres, the probability of failure of one M-bundle under far-field load per fibre σ will be $E^{(M)}(\sigma)$. Exactly paralleling the situation of individual fibres, the M-bundle is assumed to be surrounded by $N_1 = 6$ M-bundles, each of which obeys ELS. This is sketched in Fig. 11b. The stress concentrations induced by the central broken M-bundle on the fibres in the neighbouring M-bundles will, in general, be different. For simplicity, therefore, a uniform effective stress overload is defined on fibres comprising each of the N_1 neighbouring M-bundles surrounding the failed M-bundle. The interaction between M-bundles is taken to follow HLS, with a ρ-dependent correction, $K(\rho)$. The effective stress overload on the neighbours is

$$\Omega_1' = K(\rho)\ \Omega_1. \tag{45}$$

The probability that at least one of the N_1 neighbouring M-bundles fails is $\{1 - [1 - E^{(M)}((1 + \Omega_1')\sigma)]^{N_1}\}$. Continuing thus, the probability of formation of a tight cluster of P, M-bundles, altogether comprised of $L = PM$ fibre breaks, is

$$W_P(\sigma) = \left\{E^{(M)}\left(\sigma\right)\right\} \times \prod_{p=1}^{P} \left\{1 - \left[1 - E^{(M)}\left((1 + \Omega_p')\sigma\right)\right]^{N_p}\right\}, \tag{46}$$

where,

$$\Omega_p' = K(\rho)\Omega_p. \tag{47}$$

The model predicted weakest link distribution is then

$$W_{\mathrm{HLS}}(\sigma) = \lim_{P\to\infty} W_P(\sigma). \tag{48}$$

Tight cluster growth may initiate at any of the N fibres. The strength distribution of the composite patch, $G_{\mathrm{HLS}}(\sigma)$ is then obtained by substituting Eq. (48) into Eq. (6).

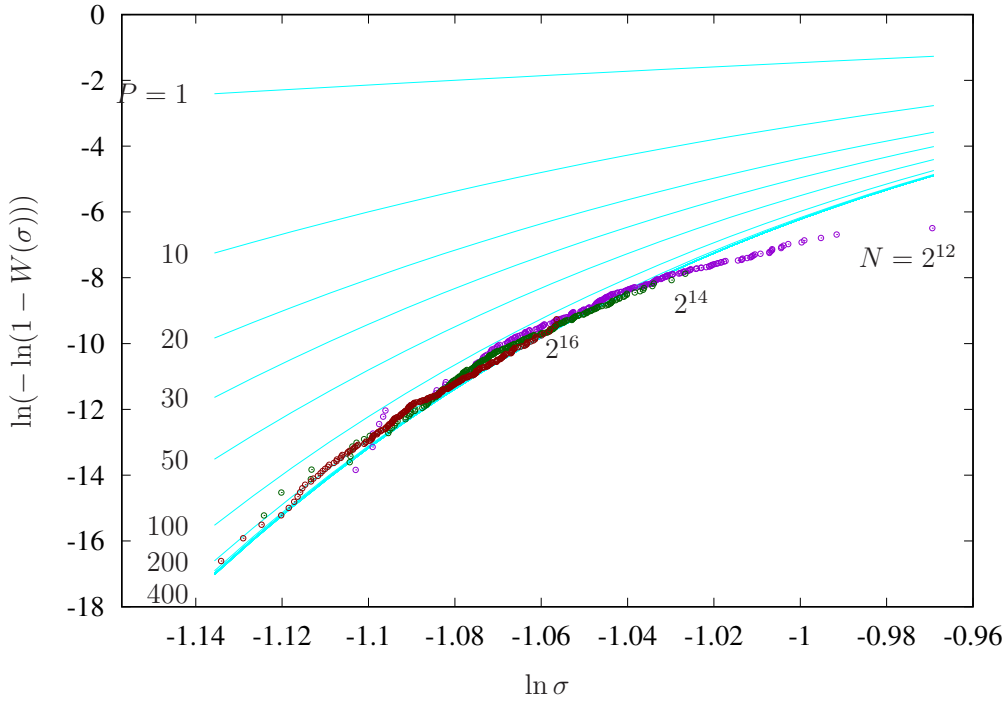

FIG. 12: Empirical weakest-link strength distribution for $\rho = 1$ and $N = 2^{12}$, 2^{14} and 2^{16}, compared with the predictions of Eq. (46) for various P.

The tight cluster growth model relates the weakest-link strength distribution of the HLS composite patch to that of smaller ELS patches, just as Curtin's scaling rule, Eq. (7), does. Excepting this similarity, the two models are conceptually very different. First, localised HLS stress overloads, Ω'_p, due to existing breaks cause new breaks in the present model. Local overloads do not feature in Eq. (7) at all. Second, the failure of an ELS M-bundle in the present model is but a part of a chain of events leading up to composite failure. The failure of an N'_c-fibre ELS bundle signifies composite failure, according to Curtin's Eq. (7). Third, the mean strength of the present M-bundles exactly equals that of an ELS bundle comprised of M fibres. This is not true for the N'_c bundles of Eq. (7). Finally, and perhaps most importantly, the number of factors, $P+1$, required for convergence will increase with decreasing σ, according to Eqs. (46) and (48). Therefore, $W_P(\sigma)$ does not scale as a power

of σ in the lower-tail. $G_{\mathrm{HLS}}(\sigma)$ will, therefore, not be Weibull distributed. On the other hand, Curtin [20] has shown that Eq. (7) leads to a Weibull distributed composite strength in the lower tail.

In fitting the parameters M and K to capture the empirical distribution functions, the focus is on fitting the lower tail of the empirical distribution. Setting the fitting parameters as $M = 24$ and $K = 0.682$ for the $\rho = 1$ composite patches yields predictions of W_P, as shown in Fig. 12. The fitting parameters are unique in that no other combination of M and K produces as good a fit of the lower tail. For sufficiently large P, which depends on σ, the $W_P(\sigma)$ converge to a curve that correctly captures the shape of the lower tail of the empirical weakest-link distribution. For example, at $\ln\sigma \approx -1.04$, $W_{P=100}$ already approximates the empirical weakest-link strength distribution well. At the lower stress-level, $\ln\sigma \approx -1.12$, however, $W_{P=100}(\sigma)$ overestimates the empirical strength distribution. $P > 200$ is needed to match Eq. (46) with the empirical strength distribution. The critical cluster that can grow catastrophically thus contains over $L = PM = 200 \times 24 = 4800$ fibres. This is larger than the Monte Carlo simulation patch sizes of most foregoing simulation studies of the present system. The largest present patch of $N = 65536$ fibres, however, comfortably accommodates the large critical cluster.

The upper tail of the empirical strength distribution is not well-captured by the tight cluster growth model. The model overestimates the failure probability in the upper tail, over the range where the empirical weakest-link strength distribution is derived from the simulation data of the $N = 2^{12} = 4096$ composite patches. This overestimation is again because the simulation patch itself is smaller than the critical cluster size ($L = PM = 4800$ fibres). Failure of small patches do not follow the dominant mechanism proposed in the tight cluster growth model. However, it must be noted that even in this range, the prediction of the tight cluster growth model is conservative.

In an entirely analogous way, the present probabilistic model is able to capture the empirical weakest link strength distribution for all $\rho > 1$. The values of M and K selected for each ρ to obtain a good fit, as shown in Fig. 9, are listed in Table I. The empirical weakest-link strength distribution obtained from the largest simulated patch size for $\rho = 0.5$ is also fit, even though it is not clear that composites larger than $N = 2^{16}$ fibres in this case obey weakest-link scaling. For $\rho \leq 5$, it is seen that the upper tail is overestimated by the probabilistic model. Again, this is because the upper tail of the empirical strength

TABLE I: Parameters of the probabilistic model of Sec. III.3 used to obtain the predicted curves shown in Fig. 9.

ρ	K	M
0.5	0.610	106
1	0.682	24
2	0.953	6
3	0.973	4
5	1.093	2
10	1.238	1

distribution is obtained from simulations on composite patches that are smaller than the critical cluster, as explained in the preceding paragraph. For $\rho = 10$, however, even the smallest simulated patch size is adequate to accommodate the small critical cluster.

III.4. Scaling of the critical cluster size

Consider next a tight cluster of P, M-bundles arranged in the form of a circular disk. In analogy with the foregoing argument, the probability of failure of an M-bundle abutting this tight cluster is given by $E^{(M)}((1+\Omega'_P)\,\sigma)$. The probability that at least one of the $N_P = 6$ M-bundles ahead of the tight cluster will fail is $1 - \left[1 - E^{(M)}((1+\Omega'_P)\,\sigma)\right]^{N_P}$. Requiring that this probability be large, say, $1 - 1/e$, results in

$$1 - \left[1 - E^{(M)}((1+\Omega'_P)\,\sigma)\right]^{N_P} = 1 - e^{-1}. \tag{49}$$

Substituting Eq. (47) into Eq. (49) results in an equation relating P and σ. For each P, this equation is readily solved for σ by the method of successive bisection.

The scaling of the critical cluster size, MP with σ is shown in Fig. 13, as predicted by the above calculation for different ρ. For clarity, attention is restricted to only those P, which correspond to circular clusters of breaks of radii $R = 1, 3, 5, \ldots$. For these clusters, the number of most overloaded intact neighbours $N_P = 6$. In the limit of small σ, $L = MP$, the criticial cluster size scales approximately as σ^{-4} with the scaling exponent gradually but systematically decreasing with decreasing ρ.

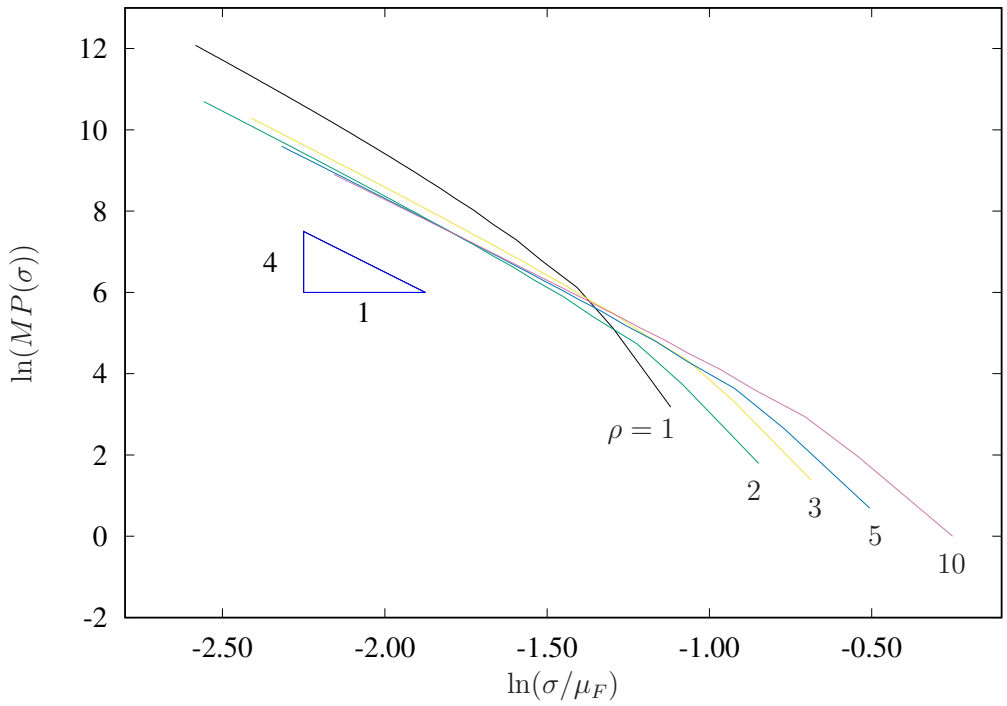

FIG. 13: Scaling of the critical cluster size, $L = PM$ with applied stress σ. For small σ, the critical cluster size scales approximately as σ^{-4}, with only a weak dependence on ρ.

IV. DISCUSSION

The statistics of Hedgepeth and Van Dyke [17] composite failure when ρ is large is well-understood in the literature [6, 19, 33, 40, 41]. The present work extends this understanding to low ρ. Monte Carlo simulations of large patches containing up to 2^{16} fibres confirm that composite strength has a weakest-link structure for $\rho \geq 1$. For $\rho < 1$ too, it appears that the weakest-link structure will prevail if even larger patches were simulated.

Commercial synthetic fibres seldom have Weibull exponents, $\rho < 5$. Natural fibres, such as sisal, jute, and coir typically have smaller Weibull exponents, approximately ranging between 2–4 [42]. The regime $\rho < 2$ is also of technological interest, as in the following case. Consider a hybrid composite, wherein different fibre types of comparable stiffness are used to reinforce the matrix, e.g., flax, and E-glass reinforced epoxy [43, 44]. The strength distribution of a typical fibre is now given by

$$F_e(\sigma) = \sum_{i=1}^{I} p_i \left(1 - \exp\left[-\left(\frac{\sigma}{\sigma_{0i}}\right)^{\rho_i}\right]\right). \tag{50}$$

Here, I is the number of types of fibres, ρ_i and σ_{0i} are the Weibull exponent and scale factor

of fibre type i, respectively. p_i is the number fraction of fibre type i, which satisfies $\sum_i^I p_i = 1$. Hybrid reinforcement increases variability of fibre strengths. This causes substantial improvement in the composite toughness, and is particularly effective in the case of natural fibre composites [45]. The variability of fibre strengths amongst all fibre types will be greater than that amongst each fibre type. If $F_e(\sigma)$ were approximated by a Weibull distribution, the effective Weibull exponent, ρ in Eq. (1), would represent the variability of fibre strengths amongst all fibre types. The equivalent ρ may then satisfy $\rho \leq \min_{i\in 1,2,\ldots,I} \rho_i$. Taking typical values for the fibre strength parameters corresponding to the flax/E-glass composite [42, 44], including $\rho_1 = 2$ and $\rho_2 = 6$, and $p_1 = p_2 = 0.5$, results in an effective $\rho \approx 0.6$ for the hybrid composite.

As noted in Secs. I.3 and I.4, brittle failure entails the development of a sufficiently large cluster of L breaks, which can propagate catastrophically. Two models, one developed presently, and another obtained from the literature are able to predict the generation of such a cluster in good agreement with the empirical Monte Carlo results. They are discussed below.

IV.1. The present weakest-link model

A tight cluster growth model, extending the model developed by Smith *et al.* [7] for LLS patches, fits the empirically obtained weakest-link strength distribution well. In this model, the weakest-link event is visualised as the occurrence of a sequence of sub-events. In the stochastic model proposed by Smith *et al.* [7] for LLS bundles, the sub-events were the failure of the intact fibres neighbouring a tight cluster of breaks. For large ρ, the variance of fibre strengths is small, and the probability of failure of one of the most overloaded fibres surrounding a tight cluster of breaks is overwhelmingly greater than that of failure of any other fibres. However, for small ρ, the variance of fibre strength is lower, and the probability of failure of any of the fibres neighbouring the cluster, not even necessarily abutting it, becomes comparable. The sequence of sub-events in the weakest-link model of Smith *et al.* [7] then are not the dominant ones. This causes the Smith *et al.* [7] model to break down at smaller ρ. This difficulty is addressed in the present model, using a devise developed by Habeeb and Mahesh [15] for LLS patches. Presently, each sub-event in the sequence of events leading to failure is the failure of an M-fibre equal load sharing (ELS) bundle. The

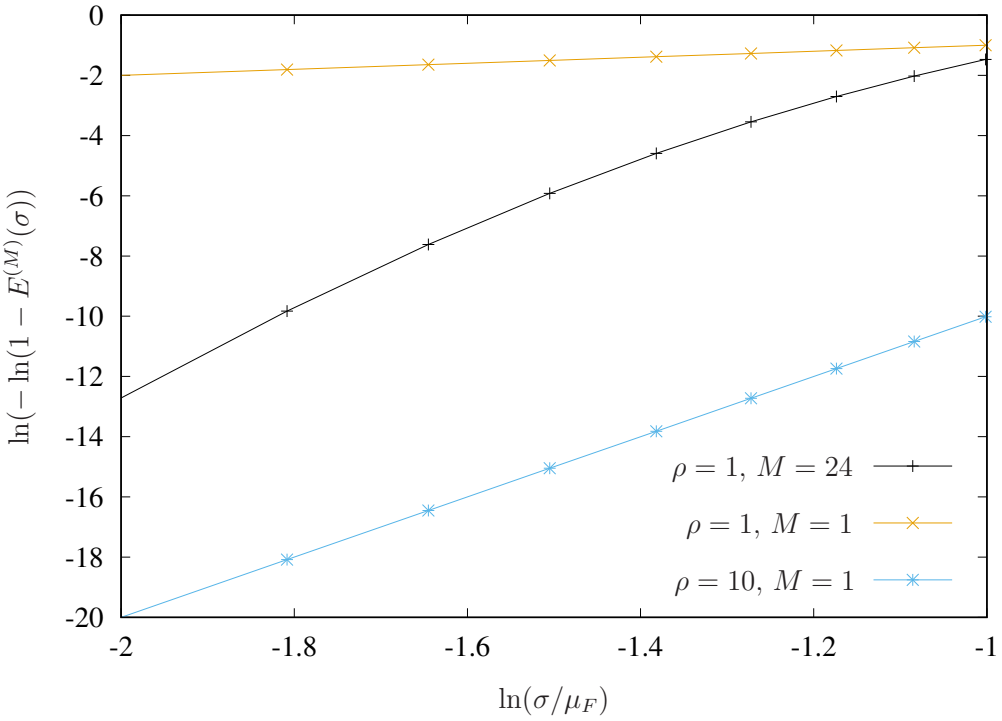

FIG. 14: Fibre and ELS m-bundle strength distributions corresponding to $\rho = 1$ and $\rho = 10$. Note that the m-bundle corresponding to $\rho = 10$ is comprised of $M = 1$ fibre only (Tab. I).

size of the ELS bundle, M, depends on ρ, as listed in Table I. For $\rho = 10$, $M = 1$, i.e., the ELS bundle is comprised of only a single fibre, and thus, the present model coincides with that of Smith *et al.* [7], adapted for HLS bundles. For decreasing ρ, however, the ELS bundles contain an increasingly large number of fibres, M. According to Tab. I, the failure of a $\rho = 1$ composite patch occurs by the growth of a tight cluster of ELS bundles, each comprised of $M = 24$ fibres.

Fig. 14 shows the strength distribution of a single fibre with $\rho = 1$, and also that of an ELS bundle consisting of $M = 24$ fibres. Similarly, the $\rho = 10$ fibre strength distribution function is also shown. The slope of these curves qualitatively indicates the scatter in fibre strengths, with smaller slopes corresponding to greater scatter. It is seen that while the $\rho = 1$ and $\rho = 10$ fibre strength distributions ($M = 1$) have widely different slopes, the $\rho = 1$, $M = 24$ and $\rho = 10$, $M = 1$ ELS bundle strength distributions have similar slopes.

The devise of identifying the failure of ELS M-bundles with the sub-events leading up to composite failure thus substantially decreases the variability in the probability of occur-

rence of the sub-events leading up to composite failure. This has the desirable consequence of making the failure of the most overloaded M-bundle neighbouring a cluster of breaks overwhelmingly most probable, as in the model of Smith *et al.* [7].

IV.2. Curtin's weakest-link model

TABLE II: Parameters N_c' and μ' used to fit the empirical strength distributions to Eq. (7).

ρ	Critical cluster size, N_c'	mean strength, μ'
0.5	30638	0.532
1	2690	0.356
2	521	0.415
3	268	0.481
5	135	0.579
10	59	0.716

The empirical strength distributions obtained from the present Monte Carlo simulations are compared with the fits obtained using the scaling relation, Eq. (7), proposed by Curtin [20] in Fig. 15. It is seen that the scaling relation fits the empirical distributions very well. This result confirms and extends the observation of Curtin [20] to lower ρ and larger patch sizes, N.

To obtain the fitting parameters N_c', and μ', the empirical strength distributions were plotted on Gaussian probability coordinates. For each $N_c' \in \{1, 2, \ldots\}$, the slope of a straight line that fits the empirical strength distribution best, in a minimum least squares sense, is computed. The reciprocal of this slope is compared with the standard deviation of Daniels' distribution, Eq. (3b). The N_c' for which the reciprocal of the slope of the straight line deviates minimally from that given by Eq. (3b) is selected. It is listed for each ρ in Table II. The mean strength, μ', is then adjusted to minimise the error between the empirical strength distributions and the model predictions. μ' is also listed in Table II.

The fitting parameters listed in Table II are not unique. Over a wide range of values of N_c', comparably good fits of the empirical distribution can be obtained. For example, Fig. 16 shows that good fits of Eq. (7) can be obtained for the empirical strength distribution for

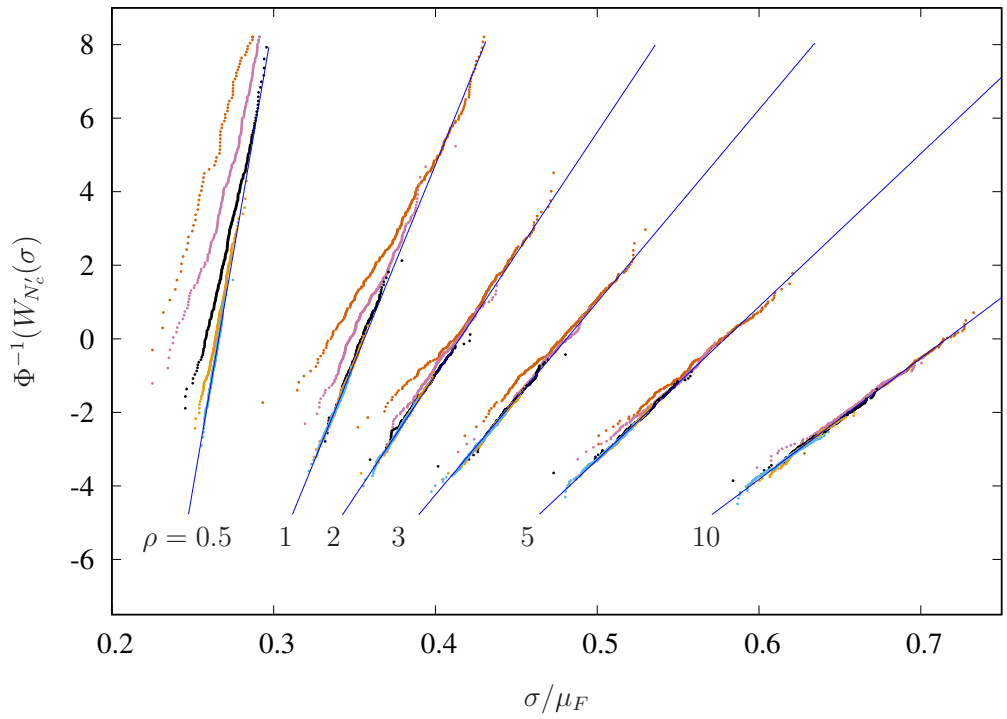

FIG. 15: Fits of the empirical strength distributions (dots) by the model (lines), Eq. (7), proposed by Curtin [20]. Fitting parameters, N'_c and μ' are listed in Table II. Vermilion, purple, black, orange and blue dots, correspond respectively to patch sizes $N \in \{2^8, 2^{10}, 2^{12}, 2^{14}, 2^{16}\}$.

$\rho = 1$ patches with $N'_c = 2000$ or 3000. In fact, for any intermediate value of N_c also, the data is fit well by Eq. (7). This contrasts with the uniqueness of the fitting parameters, M and K, in the tight cluster growth model of Sec. III.3.

The size effect predicted by the present weakest-link model, Eq. (48) is compared with that predicted by Eq. (7), due to Curtin [20] in Fig. 17. Let $\sigma_c(N)$ be the strength of a composite patch comprised of N fibres corresponding to $G_{\text{HLS}}(\sigma_c) = 1 - \exp(-1)$. Then, Eqs. (7) and (48) imply that

$$1 - \left\{1 - \Phi(\sigma_c; \mu', s_{N'_c})\right\}^{N/N'_c} = 1 - e^{-1}, \text{ and} \tag{51a}$$

$$1 - (1 - W_{\text{HLS}}(\sigma_c))^N = 1 - e^{-1}. \tag{51b}$$

It is straightforward to numerically invert both equations in Eq. (51) to obtain σ_c. Fig. 17 plots the relationship between σ_c to N, thus obtained. It is clear that both models predict nearly the same size-scaling for large N.

Surprisingly, despite the differences noted below Eq. (48) between the tight cluster growth

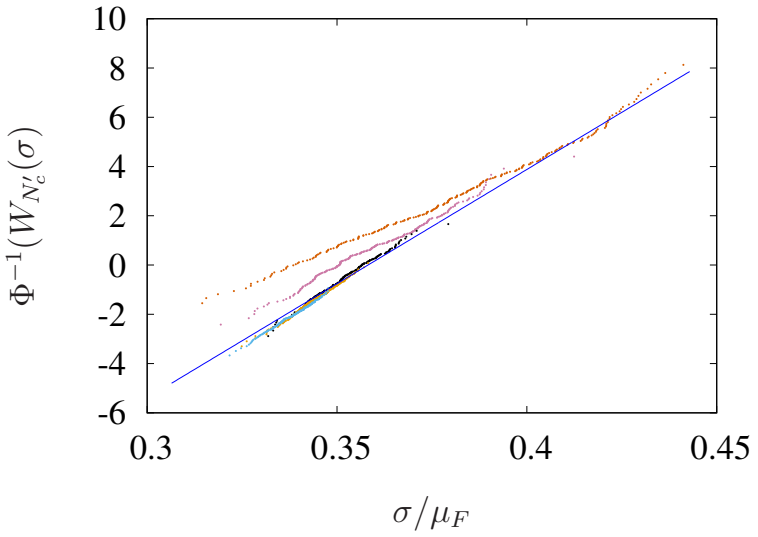

(a) $N'_c = 2000$

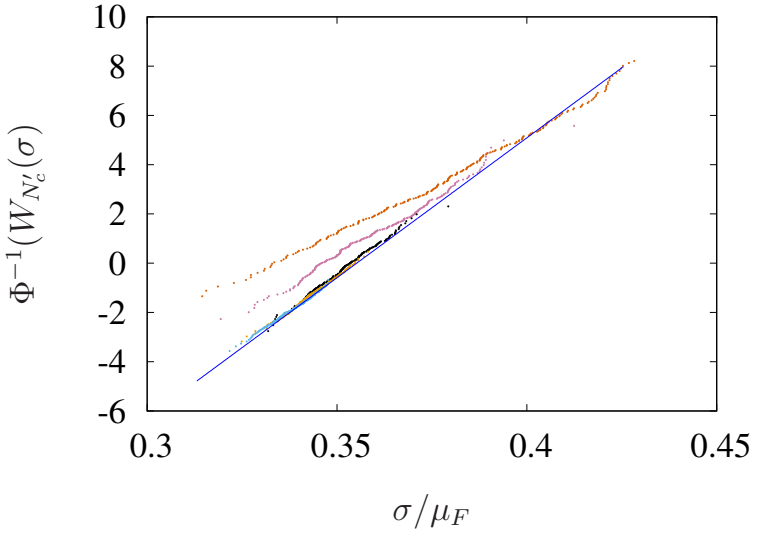

(b) $N'_c = 3000$

FIG. 16: Fits of the empirical strength distributions for $\rho = 1$ composite specimen obtained from Monte Carlo simulation using the scaling law, Eq. (7), due to Curtin [20] assuming (a) $N'_c = 2000$, and (b) $N'_c = 3000$. The mapping between colours and patch sizes is as in Fig. 15.

model, and Curtin's empirically successful scaling law, Eq. (7), their predictions coincide deep into the lower tail. A physical reason for this coincidence is not clear.

It is also known that the coincidence depends on the assumed load sharing law. In the case of the severely local LLS law, Habeeb and Mahesh [15] showed that the tight cluster

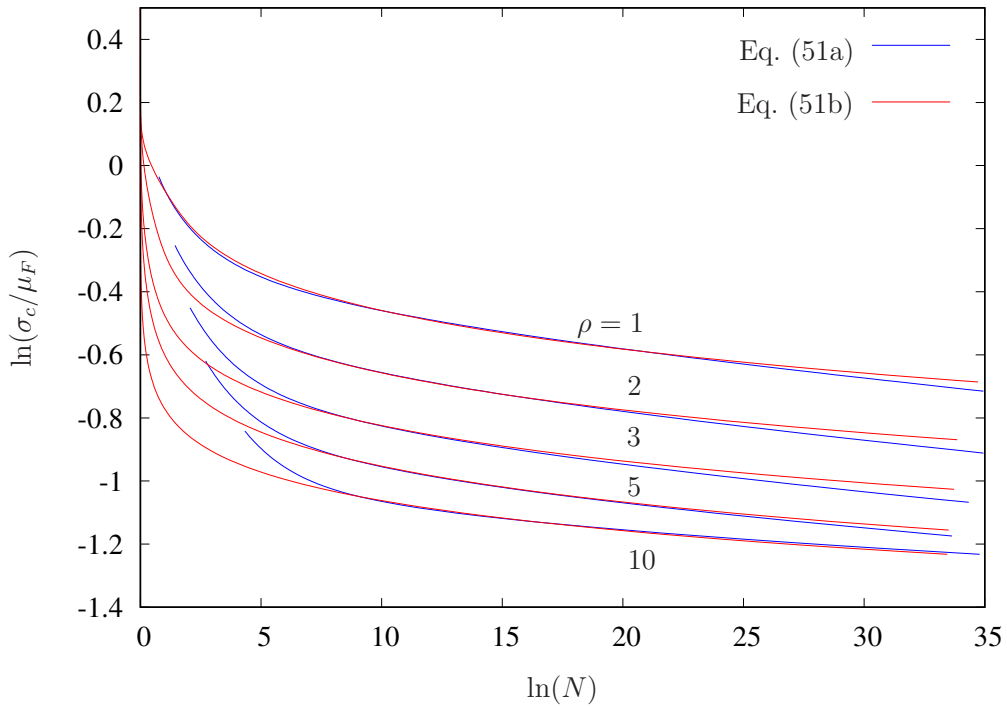

FIG. 17: Size effect predicted by Curtin's scaling law, Eq. (51a), and by the present model, Eq. (51b), for HLS composite patches.

growth model fits the empirical strength data, while Curtin's empirical scaling law does not. In the case of ELS, both the tight cluster growth model and Curtin's empirical scaling law are trivially valid by taking $M = N_c = N$. Therefore, it is speculated that for load sharing schemes that are more global than HLS, both models can capture the empirical strength distributions.

V. CONCLUSIONS

A tree based algorithm has been employed to speed up Monte Carlo failure simulations of composite patches obeying a realistic load sharing scheme. The simulations, performed on composite patches comprised of up to 2^{16} fibres, reveal the absence of a tough to brittle transition in 2-dimensional hexagonal patches. A weakest-link strength distribution underlies the composite patch strength for all ρ. A simple stochastic two-parameter model based on failure by tight growth of a cluster of breaks has been proposed. This model captures the lower tail of the empirical weakest-link strength distribution obtained from the simulations. The present model's predictions are found to coincide closely with those obtained from the

scaling-law observed by Curtin [20].

ACKNOWLEDGMENTS

The authors thank the High Performance Computing Centre at IIT Madras, where the simulations reported here were performed. We also gratefully acknowledge helpful comments from the referees.

Appendix A: Inter-nodal overload coefficients, $\Lambda_{[k][l]}$

Consider an arbitrary pair of nodes $[a]$ and $[b]$, such that $\ell_{[a]} = \ell_{[b]}$. Let these nodes be distant, in the sense that Eqs. (19) and (20) are both satisfied. A smearing function, $f(\underline{\lambda}_{[a][b]}, \overline{\lambda}_{[a][b]})$, was introduced in Eq. (21). Let

$$f(\underline{\lambda}_{[a][b]}, \overline{\lambda}_{[a][b]}) = \underline{\lambda}_{[a][b]}. \tag{A1}$$

Then, it follows from Eq. (26) that for any pair of broken fibres k_i and k_j,

$$\lambda_{k_i k_j} \geq \tilde{\lambda}_{k_i k_j}. \tag{A2}$$

The choice in Eq. (A1) thus underestimates the overload on broken fibres and is hence, not conservative. It also follows from Eqs. (12) and (A2) that

$$\sum_{\substack{k=1 \\ k \neq k_i}}^{N} \tilde{\lambda}_{k k_i} \leq 1. \tag{A3}$$

Physically, this indicates that load may be lost from the composite patch as a consequence of smearing.

If, on the other hand, the smearing function were to take the form

$$f(\underline{\lambda}_{[a][b]}, \overline{\lambda}_{[a][b]}) = \overline{\lambda}_{[a][b]}, \tag{A4}$$

overloads due to broken fibres will be overestimated, and the total load in the cross-section $\zeta = 0$ may increase due to smearing.

Non-conservation of the cross-sectional load makes both the extreme choices for the smearing function, Eqs. (A1) and (A4) unacceptable. An acceptable choice is obtained by taking

$$\Lambda_{[a][b]} = f(\underline{\lambda}_{[a][b]}, \overline{\lambda}_{[a][b]}) = s^{(\ell_{[a]}-1)} \overline{\lambda}_{[a][b]}, \tag{A5}$$

and by fixing the scalar $s \in (0, 1]$ to ensure the conservation of overload due to fibre breaks. Letting k denote a generic fibre, and letting k_1 be a broken fibre, this implies:

$$\sum_{\substack{k=1 \\ k \neq k_i}}^{N} \tilde{\lambda}_{kk_1} = 1. \tag{A6}$$

Substituting Eq. (26) into Eq. (A6) yields

$$\sum_{\ell=1}^{L} \sum_{\substack{[k] \in \mathscr{D}_{[r]}^{(\ell)} \\ [k] \neq [k_1]}} 4^{(\ell-1)} \Lambda_{[k][P_{[k_1]}^{(\ell)}]} = \sum_{\ell=1}^{L} \sum_{\substack{[k] \in \mathscr{D}_{[r]}^{(\ell)} \\ [k] \neq [k_1]}} (4s)^{(\ell-1)} \overline{\lambda}_{[k][P_{[k_1]}^{(\ell)}]} = 1. \tag{A7}$$

Here, $4^{\ell-1}$ is the number of fibres in a node of level ℓ. Eqs. (21) and (A5) have been used in the second step of Eq. (A7). Assuming a break at the fibre with coordinates $(m, n) = (0, 0)$, i.e., $k_1 = 1$, this equation can be solved efficiently for s using the method of successive bisection. For $\theta = 0.5$, and $N = 2^{16}$, it is found that $s = 0.85$.

Comparing Eqs. (A1) and (A3) on the one hand, with Eqs. (A5) and (A7) on the other also shows that

$$\underline{\lambda}_{[a][b]} \leq \Lambda_{[a][b]} = s^{(\ell_{[a]}-1)} \overline{\lambda}_{[a][b]}. \tag{A8}$$

---

[1] W. Weibull, Journal of applied mechanics **103**, 293 (1951).

[2] D. Hull and T. Clyne, *An introduction to composite materials* (Cambridge university press, 1996).

[3] M. J. Alava, P. K. Nukala, and S. Zapperi, Advances in Physics **55**, 349 (2006).

[4] H. Daniels, Proceedings of the Royal Society of London A: Mathematical, Physical and Engineering Sciences **183**, 405 (1945).

[5] L. McCartney and R. Smith, J. Appl. Mech **50**, 601 (1983).

[6] R. L. Smith, Proceedings of the Royal Society of London A: Mathematical, Physical and Engineering Sciences **372**, 539 (1980).

[7] R. L. Smith, S. Phoenix, M. Greenfield, R. Henstenburg, and R. Pitt, Proceedings of the Royal Society of London A: Mathematical, Physical and Engineering Sciences **388**, 353 (1983).

[8] D. G. Harlow and S. L. Phoenix, Journal of Composite Materials **12**, 195 (1978).

[9] D. G. Harlow and S. L. Phoenix, Journal of Composite Materials **12**, 314 (1978).

[10] W. Curtin, Journal of the Mechanics and Physics of Solids **41**, 217 (1993).

[11] D. Harlow, Proceedings of the Royal Society of London A: Mathematical, Physical and Engineering Sciences **397**, 211 (1985).

[12] P. Duxbury and P. Leath, Physical Review B **49**, 12676 (1994).

[13] S. Mahesh and S. Phoenix, Physical Review E **69**, 026102 (2004).

[14] B. Kahng, G. Batrouni, S. Redner, L. De Arcangelis, and H. Herrmann, Physical Review B **37**, 7625 (1988).

[15] C. I. Habeeb and S. Mahesh, Physical Review E **92**, 022125 (2015).

[16] J. M. Hedgepeth, NASA Technical Note **TN D-882** (1961).

[17] J. M. Hedgepeth and P. Van Dyke, Journal of Composite Materials **1**, 294 (1967).

[18] A. Gupta, S. Mahesh, and S. M. Keralavarma, International Journal of Fracture **204**, 121 (2017).

[19] S. Mahesh, S. L. Phoenix, and I. J. Beyerlein, International Journal of Fracture **115**, 41 (2002).

[20] W. Curtin, Physical Review Letters **80**, 1445 (1998).

[21] L. S. Schadler, M. S. Amer, and B. Iskandarani, Mechanics of materials **23**, 205 (1996).

[22] T. Okabe, N. Takeda, Y. Kamoshida, M. Shimizu, and W. Curtin, Composites Science and Techology **61**, 1773 (2001).

[23] T. Okabe and N. Takeda, Composites A **33**, 1327 (2002).

[24] S. Mahesh, J. Hanan, E. Üstündag, and I. Beyerlein, International Journal of Solids and Structures **41**, 4197 (2004).

[25] A. Mishra and S. Mahesh, International Journal of Solids and Structures **121**, 228 (2017).

[26] L. Mishnaevsky and P. Brøndsted, Composites Science and Technology **69**, 1036 (2009).

[27] S. Behzadi, P. Curtis, and F. Jones, Composites Science and Technology **69**, 2421 (2009).

[28] Y. Swolfs, I. Verpoest, and L. Gorbatikh, Composites Science and Technology **114**, 42 (2015).

[29] Y. Swolfs, R. M. McMeeking, I. Verpoest, and L. Gorbatikh, Composites Science and Technology **108**, 16 (2015).

[30] C. M. Landis, I. J. Beyerlein, and R. M. McMeeking, Journal of the Mechanics and Physics of Solids **48**, 621 (2000).

[31] S. Mahesh, I. J. Beyerlein, and S. L. Phoenix, Physica D: Nonlinear Phenomena **133**, 371 (1999).

[32] A. Sastry and S. Phoenix, Journal of materials science letters **12**, 1596 (1993).

[33] I. J. Beyerlein, S. L. Phoenix, and A. M. Sastry, International Journal of Solids and Structures **33**, 2543 (1996).

[34] R. S. Varga, *Matrix iterative analysis*, Vol. 27 (Springer Science & Business Media, 2009).

[35] H. Suemasu, Japan Society for Composite Materials, Transactions **8**, 29 (1982).

[36] S. Pfalzner and P. Gibbon, *Many-body tree methods in physics* (Cambridge University Press, 2005).

[37] A. Greenbaum, *Iterative methods for solving linear systems* (SIAM, 1997).

[38] W. Vandevender and K. Haskell, ACM SIGNUM Newsletter **17**, 16 (1982).

[39] T. Cormen, C. Leiserson, R. Rivest, and C. Stein, *Introduction To Algorithms* (MIT Press, 2001).

[40] I. J. Beyerlein and S. L. Phoenix, Composites Science and Technology **56**, 75 (1996).

[41] C. Landis, M. McGlockton, and R. McMeeking, Journal of Composite Materials **33**, 667 (1999).

[42] M. E. A. Fidelis, T. V. C. Pereira, O. d. F. M. Gomes, F. de Andrade Silva, and R. D. Toledo Filho, Journal of Materials Research and Technology **2**, 149 (2013).

[43] Y. Swolfs, L. Gorbatikh, and I. Verpoest, Composites Part A: Applied Science and Manufacturing **67**, 181 (2014).

[44] M. Jawaid and H. A. Khalil, Carbohydrate Polymers **86**, 1 (2011).

[45] H. Fukunaga, T.-W. Chou, and H. Fukuda, Journal of Reinforced Plastics and Composites **3**, 145 (1984).